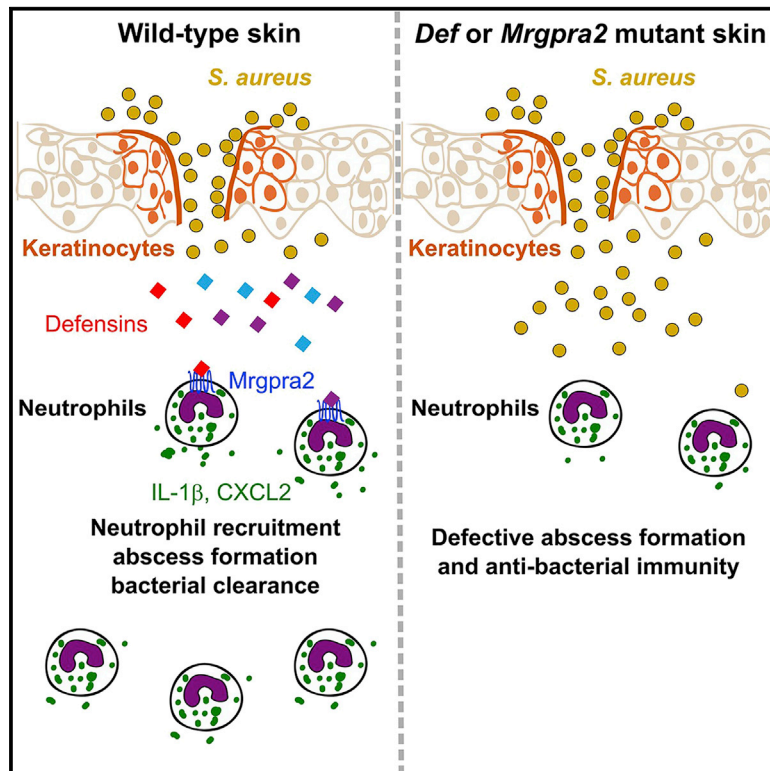


# Immunity

## Keratinocyte-derived defensins activate neutrophil-specific receptors Mrgpra2a/b to prevent skin dysbiosis and bacterial infection

### Graphical abstract



### Authors

Xintong Dong,  
Nathachit Limjunyawong,  
Elizabeth I. Sypek, ..., Brian S. Kim,  
Nathan K. Archer, Xinzhong Dong

### Correspondence

narcher2@jhmi.edu (N.K.A.),  
xdong2@jhmi.edu (X.D.)

### In brief

Antimicrobial peptides (AMPs) are vital for host defense. Dong et al. discover that keratinocyte-derived defensins activate G-protein-coupled receptors Mrgpra2a/b on neutrophils. This epithelial-neutrophil signaling axis prevents skin dysbiosis and is required for immunity against bacterial infections.

### Highlights

- Orphan GPCRs Mrgpra2a/b are defensin receptors in neutrophils
- Defensin-Mrgpra2 signaling preserves skin microbiome diversity
- Deletion of defensins or Mrgpra2 impairs neutrophil-mediated bacterial clearance
- Activation of Mrgpra2 by defensins triggers neutrophils to release IL-1 $\beta$  and CXCL2



## Article

# Keratinocyte-derived defensins activate neutrophil-specific receptors Mrgpra2a/b to prevent skin dysbiosis and bacterial infection

Xintong Dong,<sup>1,2</sup> Nathachit Limjunyawong,<sup>1</sup> Elizabeth I. Sypek,<sup>1</sup> Gaofeng Wang,<sup>3</sup> Roger V. Ortines,<sup>3</sup> Christine Youn,<sup>3</sup> Martin P. Alphonse,<sup>3</sup> Dustin Dikeman,<sup>3</sup> Yu Wang,<sup>3</sup> Mark Lay,<sup>1</sup> Ruchita Kothari,<sup>1</sup> Chirag Vasavda,<sup>1</sup> Priyanka Pundir,<sup>1</sup> Loyal Goff,<sup>1,4</sup> Lloyd S. Miller,<sup>3,7</sup> Wuyuan Lu,<sup>5</sup> Luis A. Garza,<sup>3</sup> Brian S. Kim,<sup>6</sup> Nathan K. Archer,<sup>3,\*</sup> and Xinzhong Dong<sup>1,2,3,8,\*</sup>

<sup>1</sup>The Solomon H. Snyder Department of Neuroscience, Johns Hopkins University School of Medicine, Baltimore, MD, USA

<sup>2</sup>Howard Hughes Medical Institute, Johns Hopkins University School of Medicine, Baltimore, MD, USA

<sup>3</sup>Department of Dermatology, Johns Hopkins University School of Medicine, Baltimore, MD, USA

<sup>4</sup>Department of Genetic Medicine, Johns Hopkins University School of Medicine, Baltimore, MD, USA

<sup>5</sup>Department of Biochemistry and Molecular Biology, University of Maryland School of Medicine, Baltimore, MD, USA

<sup>6</sup>Kimberly and Eric J. Waldman Department of Dermatology, Icahn School of Medicine at Mount Sinai, New York, NY, USA

<sup>7</sup>Present address: Immunology, Janssen Research and Development, 1400 McKean Road, Spring House, PA 19477, USA

<sup>8</sup>Lead contact

\*Correspondence: [narcher2@jhmi.edu](mailto:narcher2@jhmi.edu) (N.K.A.), [xdong2@jhmi.edu](mailto:xdong2@jhmi.edu) (X.D.)

<https://doi.org/10.1016/j.immuni.2022.06.021>

## SUMMARY

Healthy skin maintains a diverse microbiome and a potent immune system to fight off infections. Here, we discovered that the epithelial-cell-derived antimicrobial peptides defensins activated orphan G-protein-coupled receptors (GPCRs) Mrgpra2a/b on neutrophils. This signaling axis was required for effective neutrophil-mediated skin immunity and microbiome homeostasis. We generated mutant mouse lines lacking the entire *Defensin (Def)* gene cluster in keratinocytes or *Mrgpra2a/b*. *Def* and *Mrgpra2* mutant animals both exhibited skin dysbiosis, with reduced microbial diversity and expansion of *Staphylococcus* species. Defensins and *Mrgpra2* were critical for combating *S. aureus* infections and the formation of neutrophil abscesses, a hallmark of antibacterial immunity. Activation of *Mrgpra2* by defensin triggered neutrophil release of IL-1 $\beta$  and CXCL2 which are vital for proper amplification and propagation of the antibacterial immune response. This study demonstrated the importance of epithelial-neutrophil signaling via the defensin-Mrgpra2 axis in maintaining healthy skin ecology and promoting antibacterial host defense.

## INTRODUCTION

The skin is the largest physical and immune barrier to the external environment. Under steady-state conditions, epithelial cells and skin-resident immune cells interact with commensal micro-organisms including bacteria, fungi, and viruses and form a harmonious ecosystem (Chen et al., 2018; Grice and Segre, 2011). However, pathological disturbances can lead to an outgrowth of pathogenic bacteria such as *Staphylococcus aureus* at the cost of other diverse commensal species, a process termed dysbiosis (Byrd et al., 2018; Kobayashi et al., 2015; Nakatsuji et al., 2017; Williams and Gallo, 2017; Williams et al., 2017b). Despite the importance of microbiota in skin health, host mechanisms that prevent dysbiosis and disease remain poorly understood.

The host skin possesses an intricate immune system poised to respond to any barrier breaches and infections (Kabashima et al., 2019; Krishna and Miller, 2012; Miller and Cho, 2011; Ridder et al., 2022). Epithelial cells in the infected area are the first cells to encounter pathogens. Pathogen- and damage-

associated molecular patterns (PAMPs and DAMPs) activate pattern recognition receptors (PRRs) on keratinocytes and trigger the release of pro-inflammatory signals (Nestle et al., 2009; Pasparakis et al., 2014; Yang et al., 2017). Tissue-resident immune cells rapidly amplify the danger signal and trigger a cytokine cascade that leads to rapid recruitment of a large number of immune cells from circulation (Kim and Luster, 2015; Ley et al., 2007). Neutrophils account for the vast majority of infiltrating immune cells and are indispensable for host defense (Cho et al., 2012; Miller and Cho, 2011; Sadik et al., 2011). In response to bacterial invasion, neutrophils form an abscess around the site of infection, which effectively restricts bacterial spread and facilitates bacterial killing (Borregaard et al., 2007; Cho et al., 2012; Corbin et al., 2008; Kobayashi et al., 2018; Miller and Cho, 2011). This highly efficient defense response requires coordinated signals between the epithelial and immune cells.

Here, we report a ligand-receptor signaling axis between the skin epithelium and neutrophils that is vital for maintaining microbiome homeostasis and antibacterial immunity. The ligands are a group of epithelial cell-derived antimicrobial peptides (AMPs)



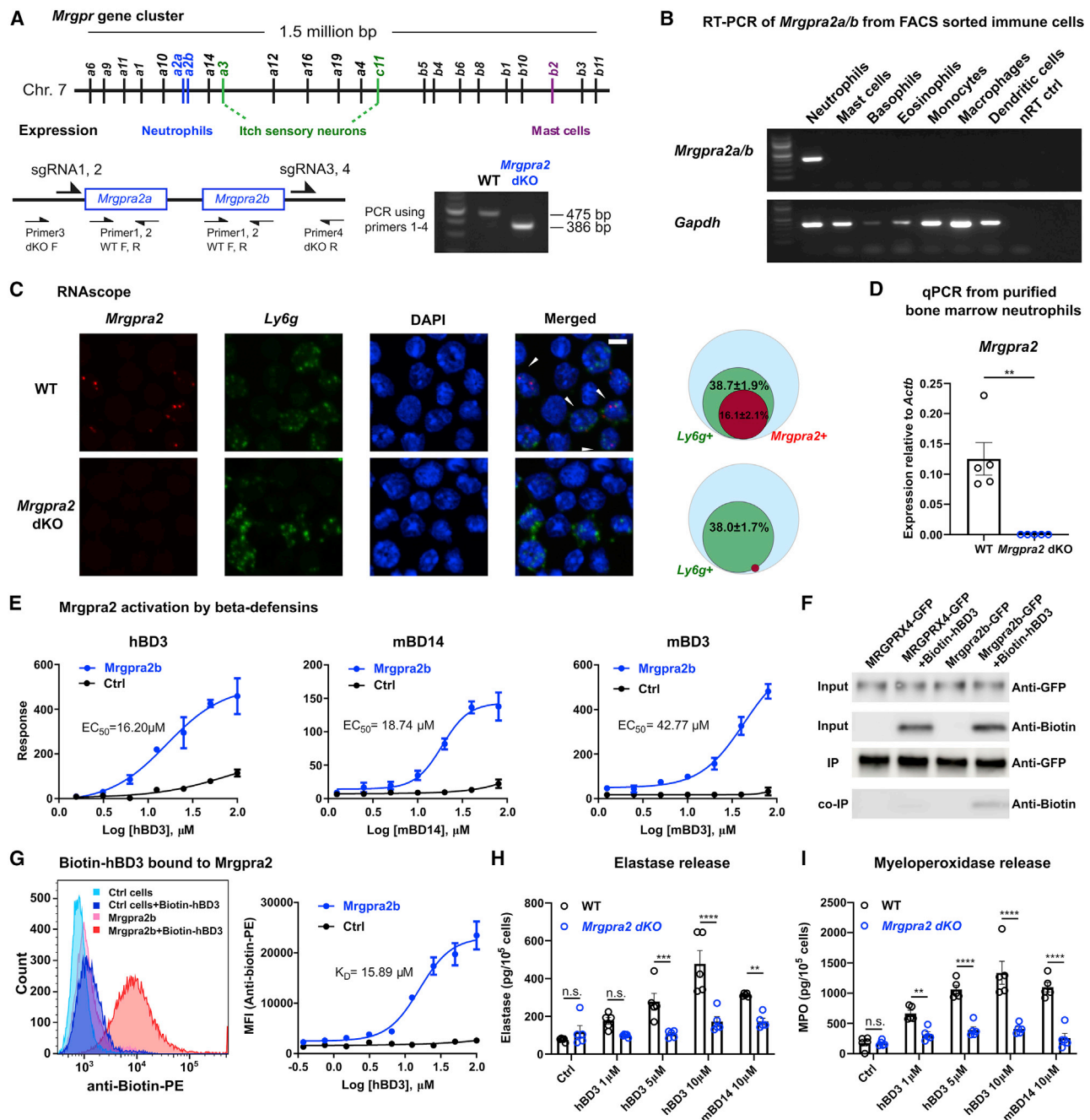


**Figure 1. *Mrgpra2a/b* were neutrophil-specific receptors for defensin**

(A) Schematic illustration of the *Mrgpr* gene cluster on mouse chromosome 7 and cellular expression specificities of a few well-studied members of the gene family. *Mrgpra2a* and *a2b* were deleted by CRISPR-cas9 using four gRNAs flanking the two genes, removing the entire genomic region. PCR genotyping using primers 1–4 as indicated in the diagram detected a WT band of 475 base pairs and an *Mrgpra2* dKO mutant band of 386 base pairs.

(B) RT-PCR gel showing expression of *Mrgpra2* and housekeeping gene *Gapdh* in FACS-sorted neutrophils, mast cells, basophils, eosinophils, monocytes, macrophages, dendritic cells, and the no reverse transcriptase control (nRT ctrl) of the neutrophil sample.

(C) Representative RNAscope *in situ* hybridization images of bone marrow cells labeled using probes for *Mrgpra2* (red), *Ly6g* (green), and DAPI (blue). Arrowheads point to *Mrgpra2*<sup>+</sup>; *Ly6g*<sup>+</sup> neutrophils. Scale bar, 5  $\mu$ m. Venn diagrams depict percentages of *Ly6g*<sup>+</sup> (green) and *Mrgpra2*<sup>+</sup> (red) cells in all bone marrow cells (blue). n = 3.

(D) qPCR of mRNA from purified bone marrow neutrophils showed that *Mrgpra2* were expressed highly in WT neutrophils but deleted from *Mrgpra2* dKO neutrophils. n = 5.

(E) HEK cells expressing *Mrgpra2b* activation by hBD3 (EC<sub>50</sub> = 16.2  $\mu$ M), mBD14 (EC<sub>50</sub> = 18.74  $\mu$ M) and mBD3 (EC<sub>50</sub> = 42.77  $\mu$ M) as determined by FLIPR intracellular calcium mobilization assay. n = 4–9.

(legend continued on next page)

named defensins. AMPs are small peptides with antibacterial, antiviral, and antifungal properties (Chessa et al., 2020; Ganz, 2003; Gerdol et al., 2020; Nakatsuji and Gallo, 2012). Defensins are the largest family of AMPs in mammalian genomes and are released by epithelial cells upon infection (Ali et al., 2001; Hinrichsen et al., 2008; Lee et al., 2005; Midorikawa et al., 2003; Miller and Cho, 2011; Pasparakis et al., 2014; Sumikawa et al., 2006). It has been shown that in addition to directly killing microbes, defensins can perform immune-modulatory functions and rapidly mobilize immune cells (Röhrli et al., 2010; Yang et al., 1999, 2017). However, due to the massive size of the gene family and highly redundant functions between members, the specific cellular and molecular mechanisms employed by defensins to orchestrate antibacterial immunity could not be evaluated in a genetic loss-of-function study (Morrison et al., 2002; Zhou et al., 2013). We overcame this problem by conditionally deleting the entire *Defensin* (*Def*) gene cluster from keratinocytes. Additionally, we identified two orphan G-protein-coupled receptors (GPCRs), *Mrgpra2a* and *Mrgpra2b*, as defensin receptors specifically expressed in neutrophils. Ablation of defensins and their neutrophil receptors both resulted in decreased skin commensal diversity and severe immune defects against *S. aureus* infections. Further, we found that defensin-*Mrgpra2* signaling mediated the release of key pro-inflammatory cytokine IL-1 $\beta$  and neutrophil autocrine chemokine CXCL2. These signals are important for neutrophil recruitment, abscess formation, and antibacterial immunity. Collectively, these findings highlighted how the defensin-*Mrgpra2* axis influenced skin ecology and critically promoted antibacterial host defense.

## RESULTS

### *Mrgpra2a* and *Mrgpra2b* were defensin receptors on neutrophils

Previously, we and others have identified members of the Mas-related GPCRs (*Mrgprs*) family (Figure 1A) as critical regulators of innate immunity (Arifuzzaman et al., 2019; Pundir et al., 2019; Subramanian et al., 2013). Expression profiling by the Immunological Genome Project Consortium revealed that mouse neutrophils express a pair of previously uncharacterized *Mrgprs*, *Mrgpra2a* and *Mrgpra2b* (Dwyer et al., 2016; Ericson et al., 2014). The two genes, which reside next to each other within the *Mrgpr* gene cluster, encode proteins that differ only by two amino acids and likely arose by duplication (Figures 1A and S1A; Sievers et al., 2011). We will refer to them together as *Mrgpra2*. Reverse transcriptase-PCR (RT-PCR) of RNA purified from fluorescence-activated cell sorting (FACS)-sorted innate immune cells confirmed that the *Mrgpra2* genes were specifically expressed by neutrophils but not by other granulocytes (mast cells, basophils, eosinophils), monocytes,

macrophages, or dendritic cells (Figure 1B). We generated *Mrgpra2a/b* double knockout (KO) (*Mrgpra2a*<sup>-/-</sup>*Mrgpra2b*<sup>-/-</sup>, referred to hereafter as *Mrgpra2* dKO) mice using CRISPR-Cas9 and confirmed deletion of *Mrgpra2* transcripts from neutrophils (Figures 1A, 1C, and 1D). *In situ* hybridization with RNAscope revealed that roughly 40% of *Ly6g*<sup>+</sup> neutrophils in wild-type (WT) bone marrow were *Mrgpra2*<sup>+</sup> (16% of total bone marrow cells, Figure 1C) and that the *Mrgpra2* transcripts were undetectable in *Mrgpra2* dKO bone marrow cells (Figure 1C). Expression of other genes in bone marrow neutrophils was not affected in the *Mrgpra2* dKO mice and neither were the percentages of neutrophils in the bone marrow, blood, and spleen in baseline conditions (Figures S1B and S1C).

Using a fluorometric imaging plate reader (FLIPR) intracellular Ca<sup>2+</sup> mobilization assay, we found that several beta-defensins activated *Mrgpra2* (Figure 1E). Human beta-defensin 3 (hBD3) and its mouse homolog mouse beta-defensin 14 (mBD14, 67% identity) evoked robust receptor activation with EC<sub>50</sub>s of 16.20 and 18.74  $\mu$ M, respectively (Figure 1E; Hinrichsen et al., 2008; Röhrli et al., 2008), while mBD3 activated *Mrgpra2* with a higher EC<sub>50</sub> (42.77  $\mu$ M) (Figure 1E). Human peptides hBD1, 2, and 4, and mouse peptides mBD1, 2, and 4 did not trigger receptor activation (Figure S1E). Raw FLIPR Ca<sup>2+</sup> traces are shown in Figure S1D. Of the four human MRGPRX receptors, MRGPRX3 was shown to be expressed in human neutrophils (Human Protein Atlas, Figure S1F) (Uhlen et al., 2019) and was activated by hBD3 at a similar EC<sub>50</sub> (10.76  $\mu$ M) (Figure S1G) but not by other human defensins tested (Figure S1H). To examine direct interaction between hBD3 and *Mrgpra2*, we synthesized N-terminal biotinylated hBD3 (biotin-hBD3), which allowed us to probe for this peptide using anti-biotin antibodies. We first used co-immunoprecipitation (coIP) to examine direct interaction between biotin-hBD3 and *Mrgpra2*. *Mrgpra2b*-GFP was pulled down using anti-GFP beads, and we found that biotin-hBD3 could be co-precipitated (Figure 1F). MRGPRX4-GFP, which was not activated by hBD3 (Figure S1G), was used as negative control. We next used a flow cytometry-based method to determine the dissociation constant ( $K_D$ ) since biotin-hBD3 bound to *Mrgpra2b*-GFP-expressing HEK cells could be detected and quantified using a PE-conjugated anti-biotin antibody (Figure 1G). We observed that hBD3 associated with *Mrgpra2b* with a  $K_D$  of 15.89  $\mu$ M, consistent with the EC<sub>50</sub> determined using the FLIPR assay (Figures 1E and 1G). Similarly, hBD3 bound to human MRGPRX3 with a  $K_D$  of 11.06  $\mu$ M, but did not bind to MRGPRX4 (Figure S1I).

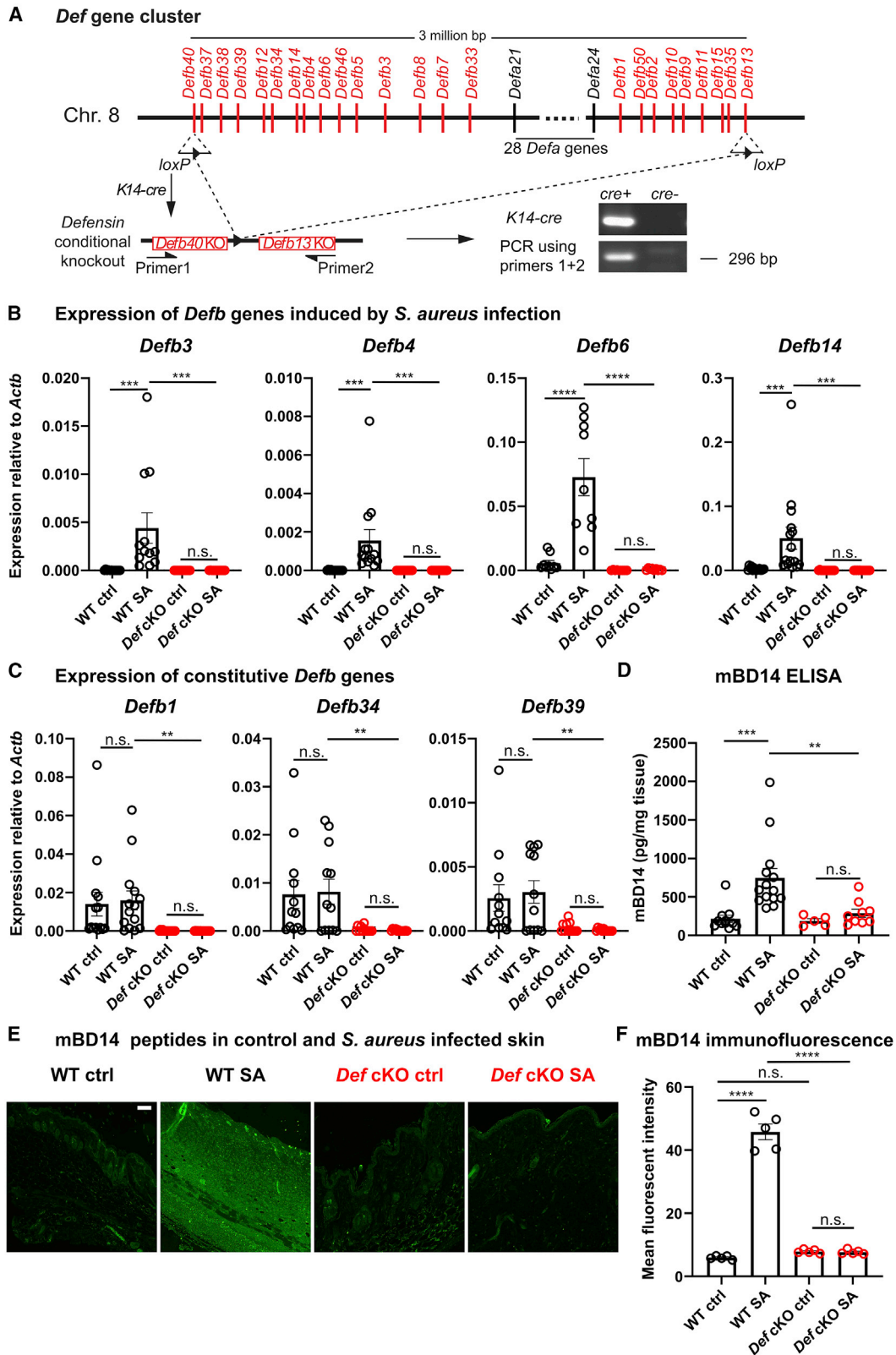
Next, we evaluated this ligand-receptor interaction by stimulating neutrophils purified from WT and *Mrgpra2* dKO mice. Neutrophils perform a variety of functions including the formation of neutrophil extracellular traps (NETs), production of reactive oxygen species (ROS), and release of granular contents

(F) Western blot showing biotin-hBD3 being co-immunoprecipitated (coIP) by *Mrgpra2b*-GFP. MRGPRX4-GFP (negative control) and *Mrgpra2b*-GFP were pulled down using anti-GFP beads, biotin-hBD3 was co-precipitated only with *Mrgpra2b*-GFP but not MRGPRX4-GFP.

(G) Dissociation constant ( $K_D$  = 15.89  $\mu$ M) between biotin-hBD3 and *Mrgpra2b* determined by flow cytometry. Left, representative flow cytometry histogram showing control HEK cells (blue) and *Mrgpra2b*-GFP-expressing cells (red) incubated with (darker shades) and without (lighter shades) biotin-hBD3 (100  $\mu$ M). Right, quantification of mean fluorescent intensity (MFI) of PE-anti-biotin showing the amount of biotin-hBD3 bound to the cells at each concentration.  $n$  = 6. (H and I) hBD3 and mBD14 triggered WT neutrophils to release elastase (H) and myeloperoxidase (I) (black). Neutrophils purified from *Mrgpra2* dKO animals did not respond to hBD3 stimuli (blue).  $n$  = 5.

Results are presented as mean  $\pm$  SEM from at least three independent experiments. \*\* $p$  < 0.01, \*\*\* $p$  < 0.001, \*\*\*\* $p$  < 0.0001, n.s. not significant by two-tailed unpaired Student's  $t$  test (D) or two-way ANOVA (H and I).

See also Figure S1.



(legend on next page)

which contain large amounts of bactericidal molecules (Mayadas et al., 2014). When applied to WT neutrophils, hBD3 did not cause chemotaxis, the formation of NETs, or ROS production (Figures S1J–S1L). However, enzyme-linked immunosorbent assay (ELISA) analysis revealed that hBD3 and its mouse homolog mBD14 triggered the neutrophils to release elastase and myeloperoxidase (MPO), two major components of primary granules (Borregaard et al., 2007; Cassatella et al., 2019; Figures 1H and 1I). Neutrophils purified from *Mrgpra2* dKO mice did not respond to hBD3 or mBD14 stimuli, suggesting that defensins activated neutrophils through *Mrgpra2* (Figures 1H and 1I). These functional assays (Figures 1E–1I), together with the expression pattern of *Mrgpra2* (Figures 1B–1D), supported the role of *Mrgpra2* as neutrophil-specific defensin receptors.

### Generation of Defensin conditional knockout mice

To investigate the roles of defensin-*Mrgpra2* interaction in skin immunity, we needed both ligand and receptor KO animals. The defensin family of AMPs can be classified into alpha- or beta- subgroups based on distinct topologies of conserved disulfide bonds (Ganz, 2003). Mouse alpha-defensins are produced by Paneth cells in the intestines (Eisenhauer et al., 1992; Salzman et al., 2003; Wilson et al., 1999), while beta-defensins are expressed and secreted primarily by keratinocytes in the skin (Ali et al., 2001; Harder et al., 2001; Midorikawa et al., 2003). More than 50 defensin-encoding genes form a 3 million-base-pair cluster on chromosome 8 in mice (Amid et al., 2009; Figure 2A). Individual defensins harbor redundant functions, making it uniquely challenging to study the functions of these important AMPs in single KO mice (Morrison et al., 2002; Zhou et al., 2013). Therefore, we sought to delete the entire *Def* cluster from the skin (Figure 2A). Using CRISPR-cas9, two *loxP* sites were inserted into the *Defb40* and *Defb13* loci, located at the two ends of the gene cluster (Figure 2A). This *Def* flox mouse (*Def<sup>flox</sup>*) was then crossed with *Keratin14-cre* (*K14-cre*) mice to conditionally KO (cKO) all *Def* genes from keratinocytes. PCR and Sanger sequencing of *K14-cre+*; *Def<sup>flox/flox</sup>* skin genomic DNA confirmed successful recombination of the *loxP* sites and removal of the *Def* gene cluster (Figures 2A and S2A).

The expressions of several *Def* genes had been shown to be induced by tissue damage or infection (Ahrens et al., 2011; Ali et al., 2001; Bals et al., 1999; Harder et al., 2001; Hinrichsen et al., 2008; Midorikawa et al., 2003; Röhrl et al., 2008; Sumikawa

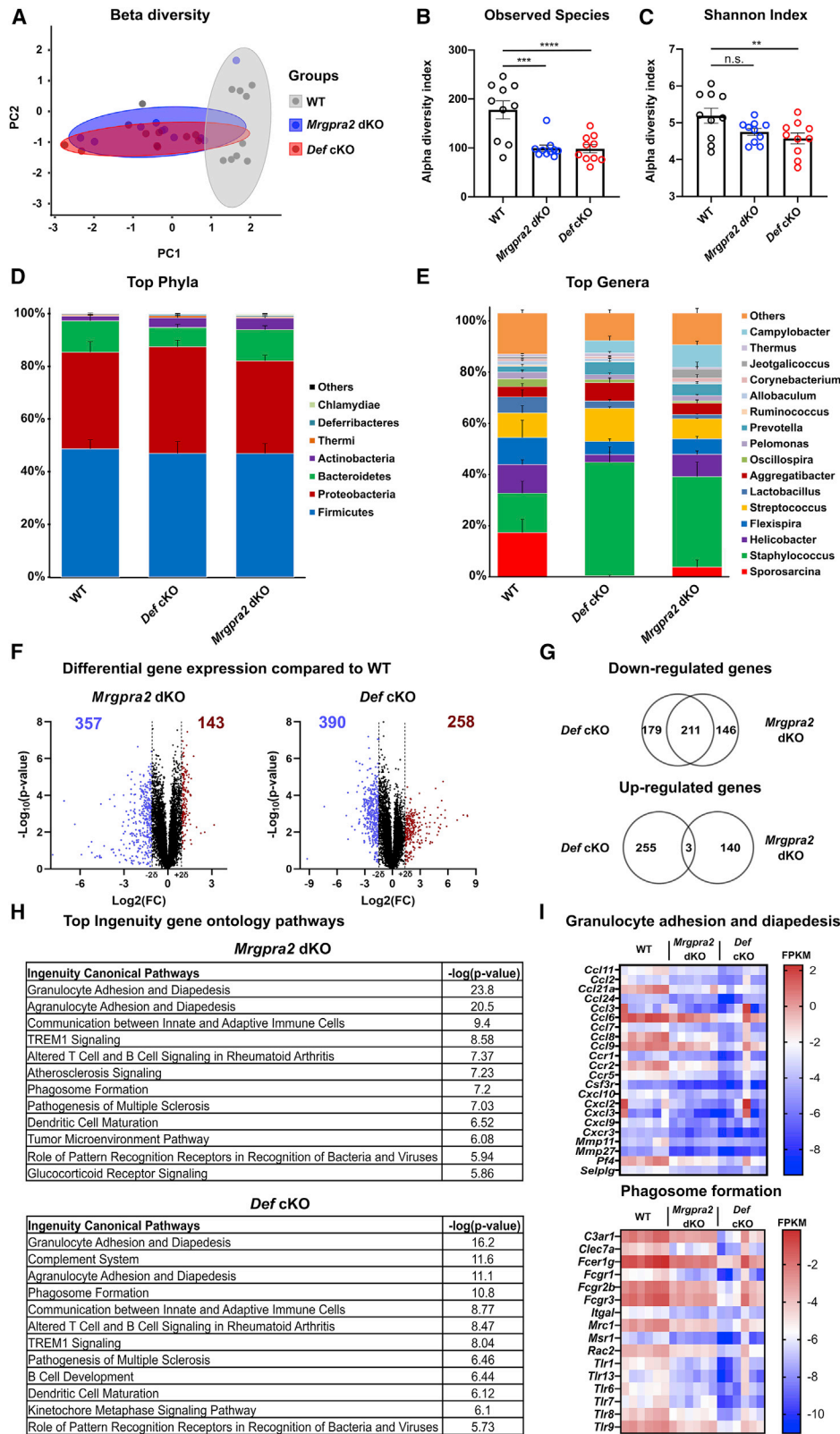
et al., 2006). To validate the deletion of *Def* genes on the mRNA level, we extracted RNA from both healthy and *S. aureus*-infected skin. We found that in WT animals, the expressions of *Defb3*, 4, 6, and 14 were robustly induced post-infection (Figure 2B), while *Defb1*, 34, and 39 were constitutively expressed in both control and infected skin (Figure 2C). RNA purified from *Def* cKO mouse skin, on the other hand, contained little or no *Defb* transcripts (Figures 2B and 2C). Consistent with previous reports (Adolph et al., 2013; Eisenhauer et al., 1992), *Defa* transcripts were not observed in the skin (Figure S2B). Further, we examined the amount of mBD14, which activated *Mrgpra2* (Figures 1E, 1H, and 1I) and was among the highest expressed beta-defensins after infection (Figure 2B; Davis et al., 2014; Harder et al., 2001; Hinrichsen et al., 2008; Midorikawa et al., 2003; Röhrl et al., 2008). Immunofluorescence staining revealed that 24 h post-*S. aureus* infection, mBD14 was observed in both epidermal and dermal areas of WT skin around the infection site, whereas infected skin of *Def* cKO mice had low amounts of mBD14 that could not be distinguished from uninfected controls (Figures 2E and 2F), as confirmed by ELISA (Figure 2D). These results showed that defensins were efficiently removed in the *Def* cKO mice on DNA, mRNA, and peptide levels.

### Disruption of the defensin-*Mrgpra2* axis caused dysbiosis and enrichment of *Staphylococcus* in the skin

Given the importance of AMPs in innate immunity, we hypothesized that defensin signaling contributed to the maintenance of skin microbiome. To directly test this hypothesis, we analyzed the skin microbiomes of WT, *Mrgpra2* dKO, and *Def* cKO animals. Littermates were weaned and genotyped at 3 weeks old then housed with other mice of the same genotype for 6 weeks under conventional housing conditions. Skin swabs were taken from the backs and analyzed using 16S rRNA sequencing (rRNA-seq) (Bolyen et al., 2019; Kozich et al., 2013). Beta diversity analyses revealed that the microbiomes of *Def* cKO and *Mrgpra2* dKO mice were similar to each other, but distinct from WT mice (Figure 3A). Alpha diversity, measured by the total number of observed species in each sample and by Shannon indices, was significantly lower in both the *Def* cKO and *Mrgpra2* dKO samples, suggesting a loss of community diversity in these mutants (Figures 3B and 3C). Phylum and genus level analyses showed that the skin of *Def* and *Mrgpra2* mutant mice were colonized by higher percentages of *Staphylococcus* (Figures 3D, 3E, and S3B), which accounted for about 12% of WT reads but 31%

### Figure 2. Generation of Defensin cluster conditional knockout mice

(A) Schematic illustration of the *Def* gene cluster on mouse chromosome 8. Two *loxP* sites were inserted into exons of *Defb40* and *Defb13* on the two ends of the gene cluster. *K14-cre*-mediated recombination successfully removed the entire 3 million-base-pair genomic region from keratinocytes. Genotyping PCR using primers flanking the cluster detected a band corresponding to partial sequence in *Defb40*, one recombined *loxP* site, and partial sequence in *Defb13*. (B and C) mRNA quantification of infection-induced *Defb3* (n = 12), *Defb4* (n = 13), *Defb6* (n = 9), and *Defb14* (n = 15) (B) and constitutively expressed *Defb1* (n = 14), *Defb34* (n = 12), and *Defb39* (n = 12) (C) in WT (black) and *Def* cKO (red) control (ctrl) skin and 24 h post-*S. aureus* infection (SA) by qPCR. The amounts of mRNA for each gene were normalized to housekeeping gene *Actb*. (D) Quantification of mBD14 peptide in control and *S. aureus*-infected skin of WT and *Def* cKO animals by ELISA. n = 5–14. (E) Representative images of mBD14 immunofluorescence of WT control skin, WT skin infected with *S. aureus*, *Def* cKO control skin and *Def* cKO skin infected with *S. aureus*. mBD14 was low in uninfected WT skin but was robustly induced 24 h after infection by *S. aureus*. In *Def* cKO animals, infection failed to induce mBD14 production. Scale bar, 100  $\mu$ m. (F) Quantification of mean fluorescent intensity of anti-mBD14 immunofluorescence across the thickness of the skin tissue as shown in (E). n = 5. Results are presented as mean  $\pm$  SEM from at least three independent experiments. \*\*p < 0.01, \*\*\*p < 0.001, \*\*\*\*p < 0.0001, n.s., not significant by one-way ANOVA. See also Figure S2.



(legend on next page)

and 36% of *Mrgpra2* dKO and *Def* cKO reads. In parallel to 16S sequencing which provided information about the relative abundance of each genus, we also used qPCR to quantify the eubacterial 16S gene as a measurement of total bacterial colonization. Compared to WT animals, the skin of both *Mrgpra2* and *Def* mutant animals contained more 16S rRNA (Figure S3A). Given the neutrophil-specific expression of *Mrgpra2*, we also evaluated the effect of systemic neutrophil depletion on the skin microbiome. WT animals were treated with an anti-Ly6G monoclonal antibody for 2 weeks, resulting in roughly 70%–80% reductions of neutrophils both in the blood and in the skin (Figure S3C). Compared to the animals that received a control antibody, anti-Ly6G treated animals displayed dysbiosis in their skin microbiome similar to the *Mrgpra2* and *Def* mutant animals (Figure S3D), with reduced community alpha diversity (Figures S3E and S3F) and increased *Staphylococcus* counts (Figure S3G). These results were consistent with our hypothesis that defensins and their neutrophil receptor *Mrgpra2* regulated skin microbiome composition. Disruption in this signaling axis resulted in dysbiosis and increased colonization by *Staphylococcus*.

To examine the cause for the difference in skin microbiome between WT and *Mrgpra2* and *Def* mutants, we used RNA sequencing (RNA-seq) to profile the entire stromal and immune landscape of the naive skin. Whole transcriptome analysis revealed down-regulation of a set of immune-related genes in both *Mrgpra2* dKO and *Def* cKO skin (Figures 3F–3I, S3H, and S3I). Ingenuity gene ontology analysis showed that the top altered pathways in both mutants include granulocyte adhesion and diapedesis and PRR signaling (Figures 3H, 3I, S3H, and S3I). The overlap in down-regulated genes between the *Mrgpra2* and *Def* KO (Figure 3G) was consistent with their ligand-receptor relationship. These observations indicated that defensins-*Mrgpra2* signaling was critical to maintaining steady baseline immunity required for a balanced and diverse skin microbiota.

In the last decade, with the advancements in microbiome analysis technologies, it has become clear that the Gram-positive pathogenic bacterium *S. aureus* is a major driver of skin dysbiosis (Kennedy et al., 2017; Meylan et al., 2017; Nakatsuji et al., 2017; Williams and Gallo, 2017; Williams et al., 2017b). We mimicked a dysbiotic scenario by topically applying *S. aureus* (SF8300 strain,  $1 \times 10^9$  colony-forming units [CFUs]) on the

surface of back skin and examined the animals' ability to restrict and eventually clear the bacteria (Malhotra et al., 2016). 18 h after epicutaneous *S. aureus* application, a significant number of Ly6G+ neutrophils could be observed in WT skin close to the epidermis and hair follicles near bacterial colonies (Figures S4A and S4B; Gallo, 2017; Lone et al., 2015; Matsumoto et al., 2021), affirming the involvement of neutrophils in clearing epicutaneous infection. *Def* and *Mrgpra2* KOs, however, had compromised responses (Figures S4A and S4B). *In vivo* imaging of bacterial luminescence revealed that the bacteria were consistently cleared by the WT skin within 4–5 days (Figures S4C and S4D). In contrast, *S. aureus* persisted until day 10 in *Def* and *Mrgpra2* mutants and led to skin lesions (Figures S4C–S4F). Collectively, changes in the mutants' steady-state microbiome composition and gene expression, as well as their inability to effectively restrict *S. aureus* on the skin surface all pointed to the importance of this epithelial-neutrophil pathway in regulating the microbial habitat.

### Defensins and *Mrgpra2* were critical for immunity against bacterial infection and abscess formation

We next analyzed the immunological deficits of the *Def* and *Mrgpra2* mutants in further detail using a well-established intradermal infection model (Miller et al., 2006; Ridder et al., 2022). In this model, a bioluminescent *S. aureus* strain (USA3000 LA-C::lux,  $3 \times 10^7$  CFU) was intradermally injected into the back skin, causing the mouse to develop a dermonecrotic lesion (Miller et al., 2007; Ridder et al., 2022; Tkaczyk et al., 2013). Co-housed animals with similar microbiomes were used in all infection studies to control for commensal variations between genotypes (Figures S5A and S5B) (Archer et al., 2019; Wang et al., 2021; Williams et al., 2017a). We monitored *in vivo* bacterial bioluminescence for 2 weeks. Throughout the course of infection, *Mrgpra2* dKO and *Def* cKO animals carried significantly higher bacterial load (Figures 4A and 4B) that spread to much larger areas (Figures 4C and 4D). Intradermal injection of human defensin hBD3 at the infection site 6 h after *S. aureus* infection was sufficient to restore the antibacterial defect of the *Def* cKO animals (Figure 4E) but did not rescue the phenotype of the *Mrgpra2* dKO animals (Figure 4F), further supporting the role of *Mrgpra2* as defensin receptors. On the other hand, adoptive transfer of purified WT neutrophils into *Mrgpra2* dKO mice 2 h

### Figure 3. *Def* and *Mrgpra2* mutant animals had altered skin microbiomes

(A–E) 16S sequencing analysis of microbial communities on the skin of WT, *Mrgpra2* dKO, and *Def* cKO mice. n = 10.

(A) Principal coordinates analysis showed that the clustering of *Mrgpra2* dKO (blue) and *Def* cKO (red) microbial communities overlapped with each other but were distinct from WT (gray).

(B) Total numbers of bacterial species observed in WT (black), *Mrgpra2* dKO (blue), and *Def* cKO (red) skin swab samples.

(C) Shannon indices of WT (black), *Mrgpra2* dKO (blue), and *Def* cKO (red) skin swab samples.

(D and E) Stacked bar charts depicting the relative abundance of top phyla (D) and top genera (E) in WT, *Mrgpra2* dKO, and *Def* cKO skin microbiota.

(F–I) RNA-seq analysis of gene expression in naive skin of WT, *Mrgpra2* dKO, and *Def* cKO mice. n = 6.

(F) Volcano plots illustrating genes with significantly down- (blue) or up-regulated (red) expression in the *Mrgpra2* dKO (left) or *Def* cKO (right) naive skin compared with WT.

(G) Top: Venn diagram showing overlap of down-regulated gene sets between *Mrgpra2* dKO and *Def* cKO. Bottom: very few overlap in the up-regulated gene sets.

(H) Top altered Ingenuity gene ontology pathways in *Mrgpra2* dKO (top) and *Def* cKO (bottom) naive skin compared with WT.

(I) Heat maps depicting fragments per kilobase per million (FPKM) mapped reads counts of genes related to granulocyte adhesion and diapedesis (top) and phagosome formation (bottom). n = 6.

Results are presented as mean  $\pm$  SEM from one experiment. \*\*p < 0.01, \*\*\*p < 0.001, \*\*\*\*p < 0.0001, n.s., not significant by one-way ANOVA.

See also Figures S3 and S4.

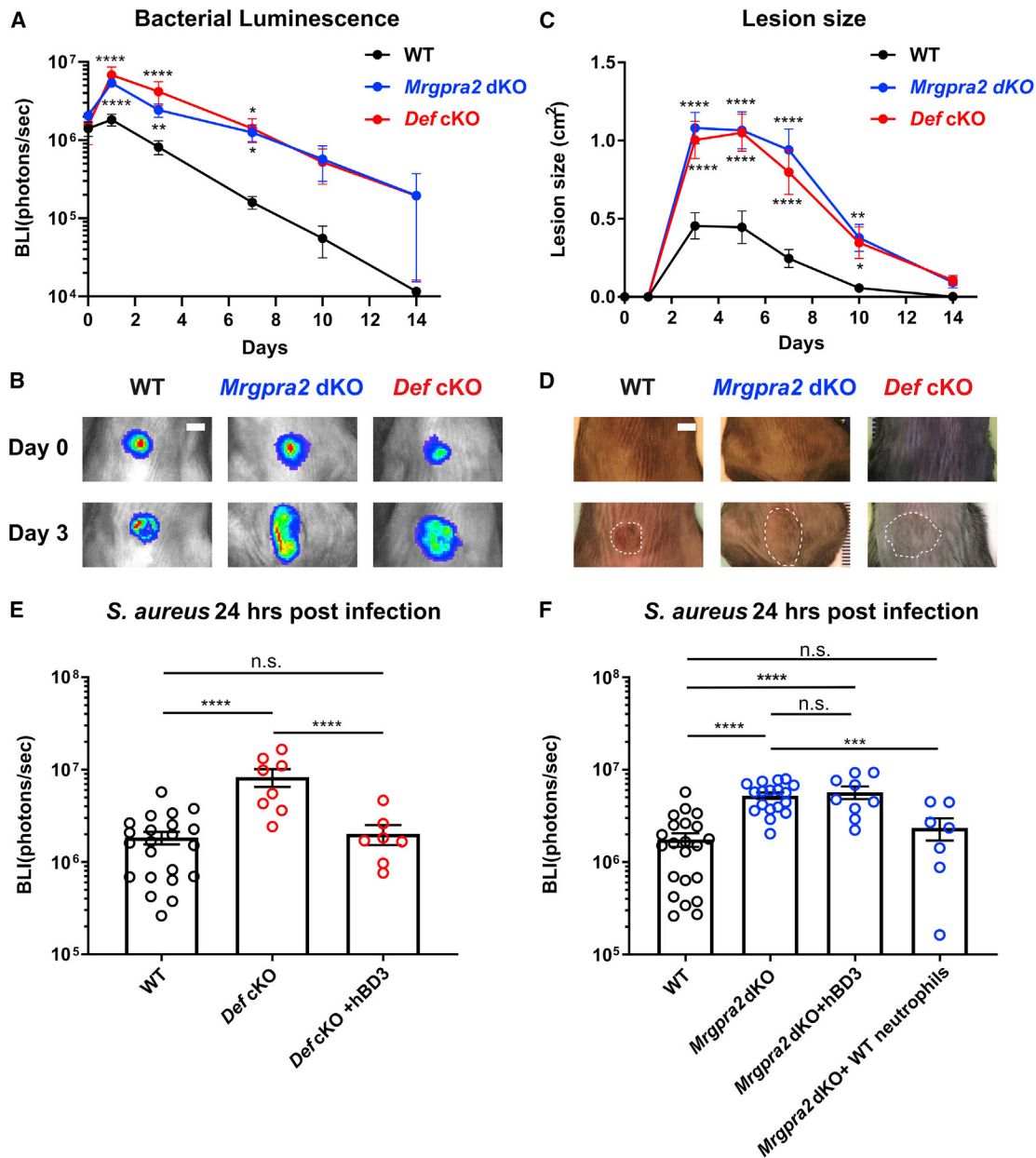


**Figure 4. *Mrgpra2* and defensins were critical for anti-*S. aureus* immunity**

(A) Bacterial luminescence (mean total flux [photons per second]) of WT (black, n = 22), *Mrgpra2* dKO (blue, n = 13), and *Def* cKO (red, n = 8) back skin intradermally infected with *S. aureus*.

(B) Representative images of *in vivo* bioluminescence. Scale bar, 0.5 cm.

(C) Mean total infected area (cm<sup>2</sup>) of WT (black), *Mrgpra2* dKO (blue), and *Def* cKO (red) back skin infected with *S. aureus*.

(D) Representative photographs of *S. aureus*-infected skin. Dotted lines indicate the demonecrotic area caused by the infection. Scale bar, 0.5 cm.

(E) hBD3 injection 6 h post-*S. aureus* infection was sufficient to rescue the antibacterial defect of *Def* cKO mice. n = 7–22.

(F) Antibacterial defect of *Mrgpra2* dKO animals could not be rescued by hBD3 injection but was fully rescued by adoptive transfer of purified WT neutrophils. n = 7–22.

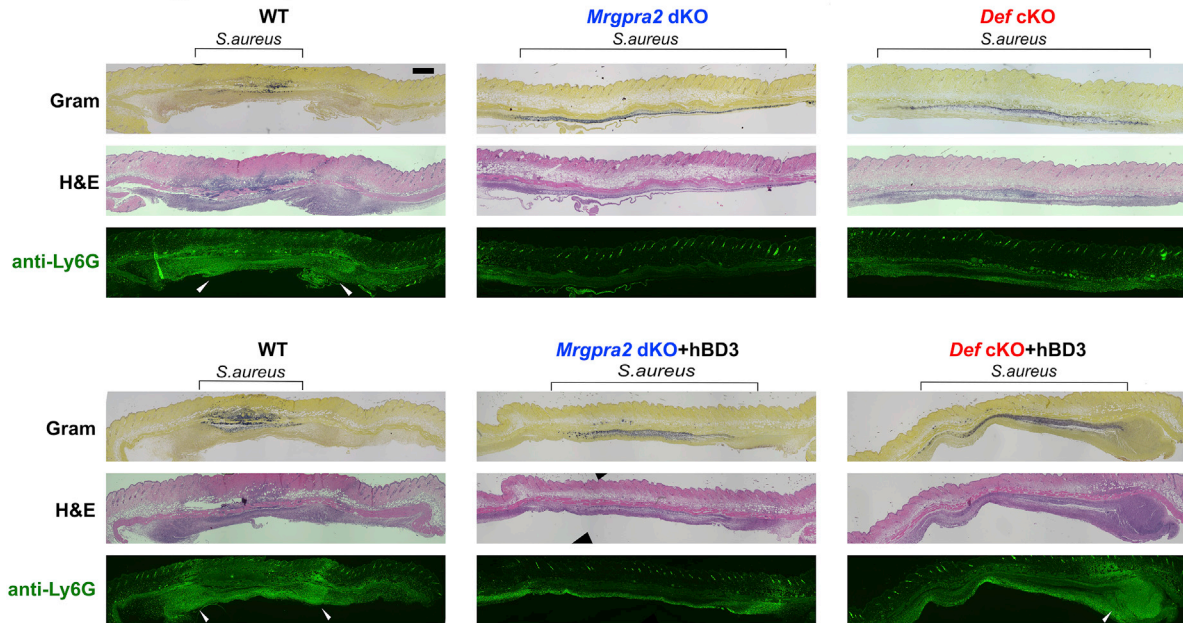
Results are presented as mean ± SEM from at least three independent experiments. \*p < 0.05, \*\*p < 0.01, \*\*\*p < 0.001, \*\*\*\*p < 0.0001, n.s. not significant by two-way ANOVA (A and C) and one-way ANOVA (E and F). In (A) and (C), comparisons were made between each mutant and WT.

See also Figure S5.

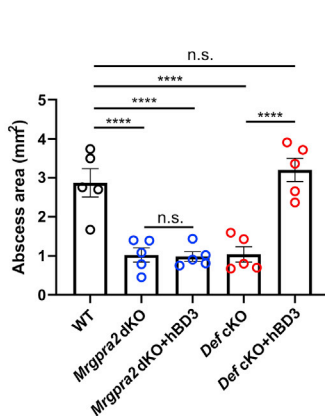
before infection fully rescued the *Mrgpra2* dKO phenotype, affirming the neutrophil-intrinsic functions of these GPCRs (Figure 4F).

The formation of a neutrophil abscess is a hallmark in anti-*S. aureus* immunity (Cho et al., 2012; Miller et al., 2006, 2007). In WT animals 24 h post-intradermal infection, staining with

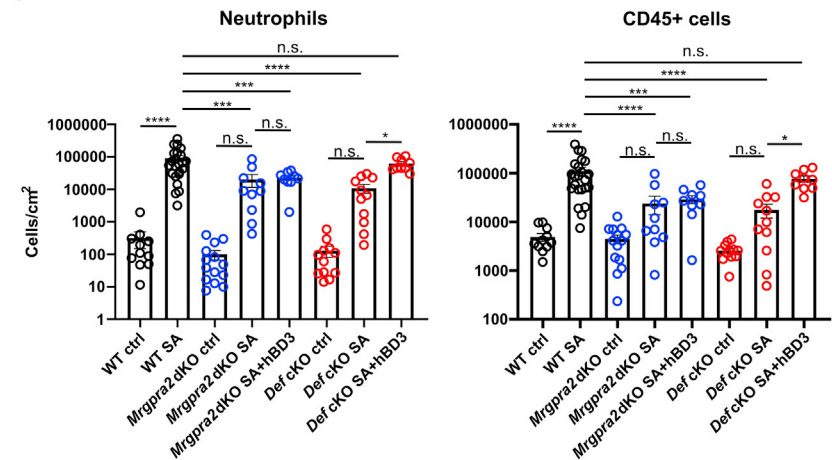
**A** Skin histology 24 hours post *S. aureus* infection



**B** Abscess area (H&E)



**C** Immune cells 24 hrs post *S. aureus* infection



**D** ELISA of neutrophil mediators

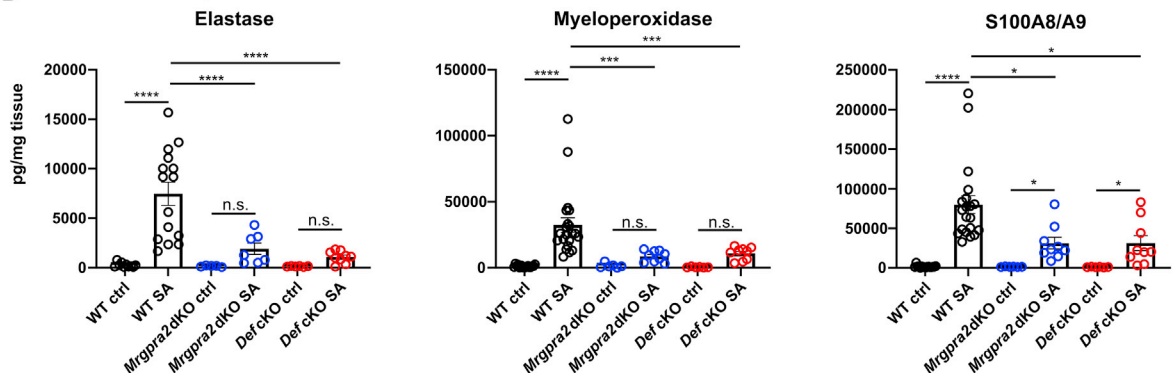


**Figure 5. *Mrgpra2* dKO and *Def* cKO animals showed severe defects in neutrophil abscess formation following *S. aureus* infection**

(A) Top row: histology staining of WT, *Def* cKO, and *Mrgpra2* dKO mouse skin 24 h post-*S. aureus* infection using Gram stain (top), H&E (middle), and immunofluorescent staining using a monoclonal antibody against Ly6G (bottom) to show the locations of neutrophils. Black brackets indicate the bacteria band. White

(legend continued on next page)

hematoxylin and eosin (H&E) and a neutrophil-specific anti-Ly6G antibody revealed large clusters of neutrophils on the edges of the infection sites, surrounding the bacteria (as shown by Gram-staining) (Figure 5A). In both *Mrgpra2* dKO and *Def* cKO animals, however, fewer neutrophils were observed, and the bacteria spread to much larger areas, consistent with the *in vivo* bacterial luminescence imaging result (Figures 4A, 4B, and 5A). The total areas of abscess formed in response to *S. aureus* infections were significantly reduced in the *Mrgpra2* and *Def* mutant animals (Figure 5B). Using flow cytometry (gating strategy in Figure S5C), we quantified the number of immune cells at the infection site 24-h post-infection. Consistent with previous reports (Cho et al., 2012), the majority of CD45<sup>+</sup> leukocytes in WT skin at this time point were neutrophils (Figure 5C). In *Mrgpra2* and *Def* mutant mice, the numbers of neutrophils in the infected skin were reduced by roughly 10-fold (Figure 5C). Consistent with the bacterial clearance phenotype (Figures 4E and 4F), injection of human defensin hBD3 was sufficient to rescue the neutrophil defects of *Def* cKO but not *Mrgpra2* dKO animals (Figures 5A–5C). The reduction in neutrophil infiltration in the infected skin of mutant animals was also evident by lower amounts of neutrophil-specific mediators (Figure 5D) including neutrophil elastase, MPO and calprotectin (S100A8/A9) (Cho et al., 2012; Corbin et al., 2008).

To acquire a comprehensive understanding of the antibacterial immune defects of the *Def* and *Mrgpra2* mutants, we performed RNA-seq of *S. aureus*-infected skin. Consistent with the neutrophil deficiencies observed by histology and flow cytometry, infected *Mrgpra2* and *Def* mutant animals exhibited altered transcriptomes characterized by a reduction in neutrophil-associated genes and pathways compared with WT (Figures 6A–6D and S6A–S6C; Ericson et al., 2014). Among the most significantly down-regulated genes in both *Mrgpra2* and *Def* mutants were pro-inflammatory cytokines *Il1a*, *Il1b* and *Tnf*, chemokines *Cxcl2* and *Ccl3*, as well as inflammasome component *Nlrp3* (Figures 6A and 6B). The expressions of several key genes were validated using qPCR (Figure S6C). Ingenuity gene ontology analysis showed that the top pathways affected in both *Mrgpra2* dKO and *Def* cKO include granulocyte adhesion and diapedesis (Figures 6C and 6D), glucocorticoid receptor signaling, Toll-like receptor signaling and IL-10 signaling, all of which are linked to inflammatory and antimicrobial responses (Figure 6C). Ingenuity also identified a network of inter-related pathways down-regulated in both mutants centering on a few key genes including the pro-inflammatory cytokine IL-1 $\beta$  (Figure S6B). We confirmed the reduced IL-1 $\beta$  in *Mrgpra2* dKO and *Def* cKO infected skin using both qPCR (Figure S6C) and ELISA (Figure S7A). This finding was particularly interesting since we know that mutant animals lacking neutrophil-derived

IL-1 $\beta$  showed very similar phenotypes to *Def* and *Mrgpra2* mutants when infected by *S. aureus*, with significantly higher bacterial burden, larger necrotic lesions, and a significant loss of neutrophil abscess (Cho et al., 2012; Miller et al., 2007). Given the neutrophil-specificity of *Mrgpra2* and the central roles of neutrophil-derived cytokines and chemokines in antibacterial immunity (Cho et al., 2012; Miller and Cho, 2011), we next sought to understand the effects of defensin-*Mrgpra2* interaction on neutrophil cell biology and to identify key effectors downstream of ligand-receptor signaling system.

### Defensin-*Mrgpra2* interaction triggered neutrophils to release IL-1 $\beta$ and CXCL2

Neutrophils are the most numerous leukocytes in circulation and can be rapidly recruited to the site of infection to kill infiltrating pathogens (Mayadas et al., 2014). Uncontrolled neutrophil activity can cause severe tissue damage, thus the activation of these cells generally follows a tightly regulated multi-step process: Upon entering the inflamed tissue, neutrophils can first become “primed” by a variety of microbial-derived PAMPs or cytokines (“signal 1”) (Figure 7B; Miralda et al., 2017; Wright et al., 2013). Priming leads to the expression of a set of cytokine and chemokines including IL-1 $\beta$ , CXCL2, CCL3, and TNF- $\alpha$  (Wright et al., 2013; Figures 7A and 7C). The primed neutrophils are now poised to respond rapidly to other activating stimuli (“signal 2”) (Figure 7B), release these pro-inflammatory molecules and perform their effector functions. Importantly, several neutrophil-derived factors were shown to primarily act on other neutrophils, thus forming an “autocrine” signal amplification loop that result in a highly coordinated immune response targeted precisely to the site of infection (Ballesteros et al., 2020; Cho et al., 2012; Chou et al., 2010; Lämmermann et al., 2013; Lentini et al., 2020; Sadik et al., 2011).

We utilized a proteome profiler array (R&D systems) to identify key cytokines and chemokines released from neutrophils in response to defensin stimuli. Human hBD3 or its mouse homolog mBD14 alone did not trigger the production or release of any cytokine or chemokine included in the array and thus did not serve as priming signals (Figures 7A and 7C–7E). We then used *S. aureus*-derived lipoteichoic acid (LTA, a Toll-like receptor 2 ligand) as signal 1 (Lotz et al., 2004). LTA stimulus alone triggered the release of more IL-1RA, CCL3, CCL4, CXCL2, and TNF $\alpha$  compared with the control (Figures 7A, 7C, and 7D). It also induced the production of IL-1 $\beta$ , but the cytokine was not released from the cells (Figures 7A and 7D). When hBD3 or mBD14 were added following LTA, we saw a significant increase in the amount of IL-1 $\beta$  and CXCL2 in the extracellular supernatant (Figures 7A, 7C, and 7D). In contrast, neutrophils purified from *Mrgpra2* dKO did not respond to hBD3 or mBD14 (Figures 7A and 7D), though the priming effects of LTA did not

arrowheads point to neutrophil abscesses. Scale bar, 1 mm. Bottom row: hBD3 injection rescued abscess formation in *Def* cKO but not *Mrgpra2* dKO mutant animals.

(B) Quantification of abscess areas based on H&E staining shown in (A).  $n = 5$ .

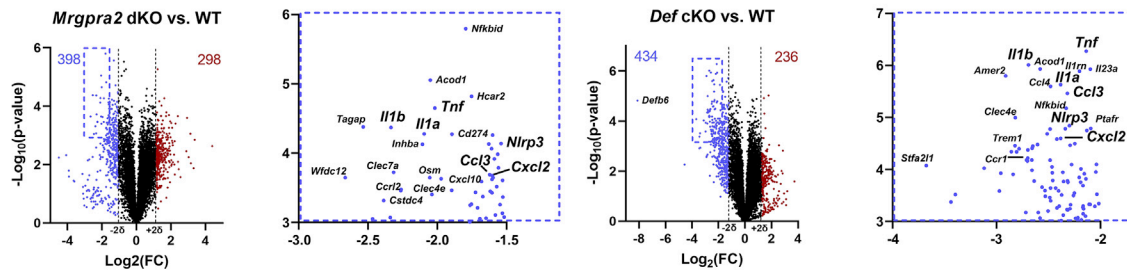
(C) Flow cytometry analyses of total CD45<sup>+</sup> cells and neutrophils in the skin 24 h post-*S. aureus* infection. Both *Def* cKO and *Mrgpra2* dKO animals showed reduced recruitment of neutrophils. hBD3 injection rescued neutrophil recruitment of *Def* but not *Mrgpra2* mutants.  $n = 9–23$ .

(D) ELISA quantifications of elastase, myeloperoxidase (MPO), and calprotectin (S100A8/A9 dimer) in the skin of WT, *Def* cKO, and *Mrgpra2* dKO mice 24 h post-*S. aureus* infection.  $n = 6–21$ .

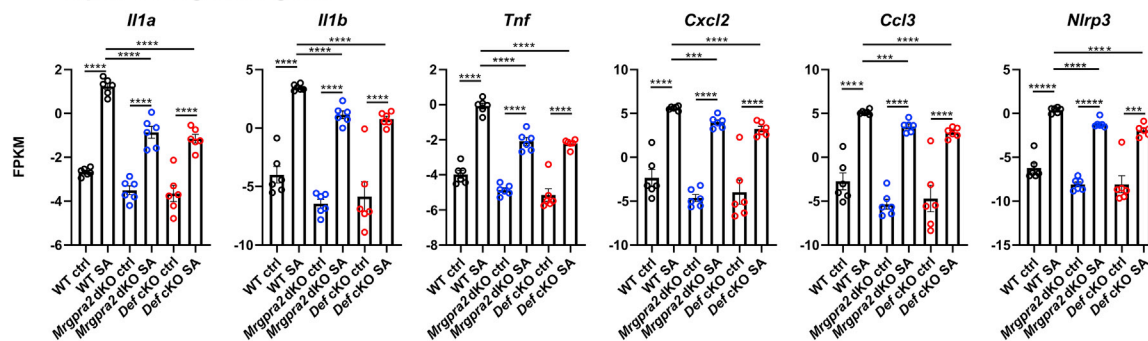
Results are presented as mean  $\pm$  SEM from at least three independent experiments. \* $p < 0.05$ , \*\*\* $p < 0.001$ , \*\*\*\* $p < 0.0001$ , n.s., not significant by one-way ANOVA.

See also Figure S5.

**A Differential gene expression post *S.aureus* infection**



**B Top down-regulated genes**



**C Top down-regulated Ingenuity pathways**

<i>Mrgpra2</i> dKO		<i>Def</i> cKO	
Ingenuity Canonical Pathways	-log(p-value)	Ingenuity Canonical Pathways	-log(p-value)
Granulocyte Adhesion and Diapedesis	9.81	Granulocyte Adhesion and Diapedesis	30.2
Glucocorticoid Receptor Signaling	8.61	Agranulocyte Adhesion and Diapedesis	20.4
Role of Hypercytokinemia/hyperchemokinememia in the Pathogenesis of Influenza	8.32	Role of Hypercytokinemia/hyperchemokinememia in the Pathogenesis of Influenza	15.8
Agranulocyte Adhesion and Diapedesis	7.17	IL-10 Signaling	14.5
Communication between Innate and Adaptive Immune Cells	6.66	Tumor Microenvironment Pathway	12
Toll-like Receptor Signaling	6.26	Communication between Innate and Adaptive Immune Cells	11.3
IL-10 Signaling	5.84	Role of Pattern Recognition Receptors in Recognition of Bacteria and Viruses	11.1
Altered T Cell and B Cell Signaling in Rheumatoid Arthritis	5.69	Role of Macrophages, Fibroblasts and Endothelial Cells in Rheumatoid Arthritis	11
LXR/RXR Activation	5.44	LXR/RXR Activation	10.8
Atherosclerosis Signaling	5.39	Altered T Cell and B Cell Signaling in Rheumatoid Arthritis	10.8
TREM1 Signaling	5.2	Glucocorticoid Receptor Signaling	10.1
LPS/IL-1 Mediated Inhibition of RXR Function	5.12	IL-17 Signaling	9.81

**D Genes related to neutrophil functions**

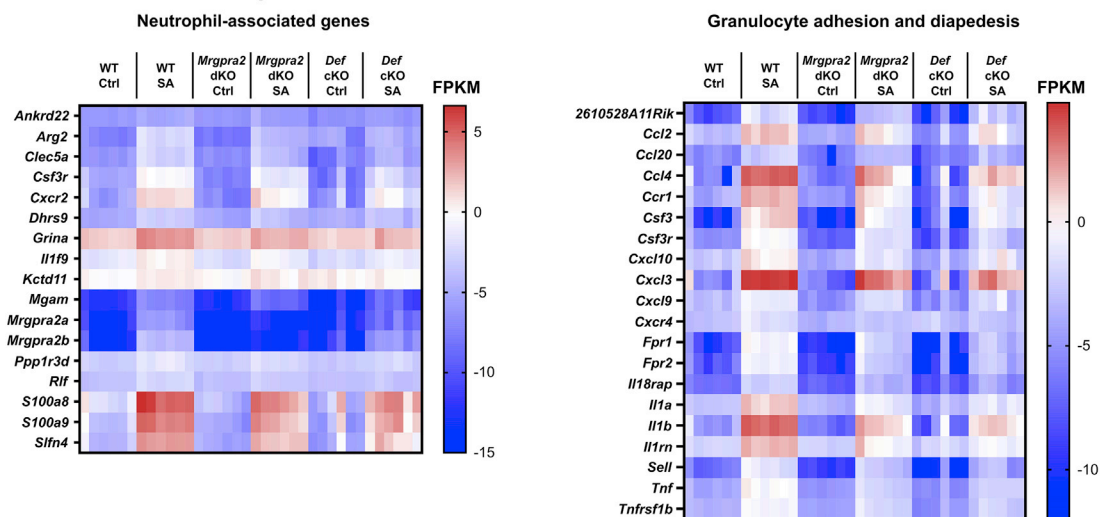


**Figure 6. RNA-seq analysis of WT, *Mrgpra2* dKO, and *Def* cKO skin 24 h post-*S. aureus* infection**

(A) Volcano plots illustrating genes with significantly down- (blue) or up-regulated (red) expression in the *Mrgpra2* dKO (left) or *Def* cKO (right) infected skin compared with WT. Boxed areas in the upper-left corners were magnified to show the most significantly down-regulated genes in detail.

(legend continued on next page)

differ between WT or *Mrgpra2* dKO neutrophils (Figures 7A, 7C, and 7D). IL-1 $\beta$  is synthesized and stored as a 31 kDa pro form in primed neutrophils and is cleaved and released as a 17-kDa mature form in an inflammasome-dependent manner (Martinon et al., 2002; Miller et al., 2007; Shi et al., 2015). We used western blot to distinguish the 31 kDa pro-IL-1 $\beta$  from the 17 kDa cleaved IL-1 $\beta$  (Figure 7E). Consistent with the proteome profiler and ELISA results (Figures 7A–7D), LTA induced the production of pro-IL-1 $\beta$  in both WT and *Mrgpra2* dKO neutrophils, but only WT neutrophils released cleaved IL-1 $\beta$  in response to hBD3 (Figures 7E and 7F), affirming the notion that defensin activated neutrophils via the *Mrgpra2* receptor. We further examined hBD3-mediated IL-1 $\beta$  release using pharmacological inhibitors. quinoline-valine-aspartic acid-difluorophenoxymethyl ketone (Q-VD-OPh), a pan-caspase inhibitor, effectively reduced IL-1 $\beta$  release from WT neutrophils in response to hBD3, indicating that the process was caspases-dependent (Figures 7E and 7F). The defensin-*Mrgpra2* ligand-receptor interaction was also inhibited by a Gq inhibitor YM-254890 (Figures 7E and 7F), consistent with informatic predictions that *Mrgpra2a/b* were Gq-coupled GPCRs (Singh et al., 2019).

Last, we tested whether injecting IL-1 $\beta$  and CXCL2 could alter the immune responses of *Mrgpra2* and *Def* mutant animals. We reasoned that, if these cytokine and chemokine were downstream of defensin-*Mrgpra2* signaling, supplying exogenous IL-1 $\beta$  and CXCL2 would rescue the anti-*S. aureus* phenotype of the mutant animals. Injection of recombinant mouse CXCL2 alone did not alter the mutant phenotypes (Figure 7G); whereas IL-1 $\beta$  (17-kDa form) alone or co-injecting IL-1 $\beta$  and CXCL2 significantly reduced the bacterial load in both *Mrgpra2* dKO and *Def* cKO animals 24 h post-infection (Figure 7G). Histological analyses of post-infection tissues also showed that IL-1 $\beta$  and CXCL2 restored the neutrophil abscess in the *Mrgpra2* and *Def* mutants (Figures 7H and 7I). These results showed that IL-1 $\beta$  and CXCL2 acted downstream of the defensin-*Mrgpra2* signaling axis. Given the importance of IL-1 $\beta$  in anti-*S. aureus* immunity (Cho et al., 2012; Miller et al., 2007) and as a downstream factor of defensin-*Mrgpra2* signaling, we were curious whether *Il1b* mutant animals also harbored altered skin microbiota. Interestingly, 16S sequencing revealed strong skin dysbiosis in the *Il1b* KO animals (Figure S7B), with drastically reduced community diversity (Figures S7C and S7D). However, unlike animals lacking defensins, *Mrgpra2* (Figure 3E) or neutrophils (Figure S3G), the skin microbiota of *Il1b* mutants were dominated by *Sporosarcina* (Figure S7E), which is a common component of the murine gut microbiome (Guo et al., 2022; Zhao et al., 2019). This was likely due to the important roles of IL-1 $\beta$  in intestinal immunity which could potentially interfere with the skin microbiome (Franchi et al., 2012; Molloy et al., 2013).

In summary, our results demonstrated that keratinocytes released defensins in response to *S. aureus* skin infections. These AMPs activated *Mrgpra2* receptors on neutrophils and triggered the release of IL-1 $\beta$  and CXCL2. Additional neutrophils

responded to these inflammatory signals, infiltrated into the tissue, released more pro-inflammatory cytokine and chemokines, and effectively propagated the immune response. Abolishing the defensin-*Mrgpra2* axis by either removing all defensin ligands from the keratinocytes or the *Mrgpra2* receptors from the neutrophils disrupted this signaling cascade and caused the severe deficiencies in abscess formation and antibacterial immunity observed in the mutants.

## DISCUSSION

Our study revealed an important epithelial to neutrophil signaling pathway that was vital for skin immunity and microbiome homeostasis. The idea that defensins both directly kill bacteria and signal to immune cells via their cell surface receptors has long been appreciated (Ganz, 2003; Röhrli et al., 2010; Subramanian et al., 2013; Yang et al., 1999, 2017). However, genetic studies of these important AMPs have been hindered by the massive redundancy of this gene family (Morrison et al., 2002; Navid et al., 2012; Zhou et al., 2013). The *Def* cKO mice allowed us to directly demonstrate the host-intrinsic immune-modulatory functions of defensins beyond direct bacterial killing. Our results clearly showed that removal of all defensins from keratinocytes resulted in severely compromised neutrophil response to infection. The importance of neutrophils in defensin-mediated immunity was further highlighted by the identification of *Mrgpra2a* and *Mrgpra2b* as neutrophil-specific defensin receptors. *Mrgpra2* dKO mice phenocopied the *Def* cKO mice in every aspect we analyzed, with similar microbiome dysbiosis, comparable defects in antibacterial immunity and a lack of neutrophil abscess formation post-infection. These results pointed to neutrophils as key effector cells of defensin signaling.

Neutrophils are the most abundant granulocytes in circulation and have been shown to be the key players in a wide range of immune functions (Cassatella et al., 2019; Mayadas et al., 2014; Miller and Cho, 2011; Sadik et al., 2011). Here, we identified a pair of receptors important for neutrophil functions. The *Mrgpr* family of GPCRs have attracted much attention as key regulators of innate immune functions (Arifuzzaman et al., 2019; Dwyer et al., 2016; McNeil et al., 2015; Pundir et al., 2019). *Mrgpra2a* and *a2b* showed highly specific expression in mouse neutrophils (Dwyer et al., 2016; Ericson et al., 2014) and were vital to antibacterial functions. Several key questions remain to be answered. First, the precise intracellular signaling pathways employed by *Mrgpra2* remain to be defined. Both bioinformatics prediction (Singh et al., 2019) and our pharmacological inhibition result suggested that *Mrgpra2a/b* were Gq-coupled GPCRs, and likely engaged Ca<sup>2+</sup> as part of the signaling cascade. Importantly, we found that in the context of *S. aureus* infections, defensins did not serve as priming “signal 1,” but rather acted on primed neutrophils as “signal 2” and that IL-1 $\beta$  and CXCL2 were key downstream effectors of defensin-*Mrgpra2* signaling. Still, the full picture of functional consequences of *Mrgpra2* activation in

(B) FPKMs of key pro-inflammatory genes in WT, *Mrgpra2* dKO, and *Def* cKO naive and *S. aureus*-infected skin. n = 6.

(C) Top altered Ingenuity gene ontology pathways in *Mrgpra2* dKO (top) and *Def* cKO (bottom) *S. aureus*-infected skin.

(D) Heat maps depicting FPKM of neutrophil-associated genes and genes related to granulocyte adhesion and diapedesis.

Results are presented as mean  $\pm$  SEM from one experiment. \*\*\*p < 0.001, \*\*\*\*p < 0.0001, \*\*\*\*\*p < 0.00001, n.s., not significant by one-way ANOVA. See also Figure S6.

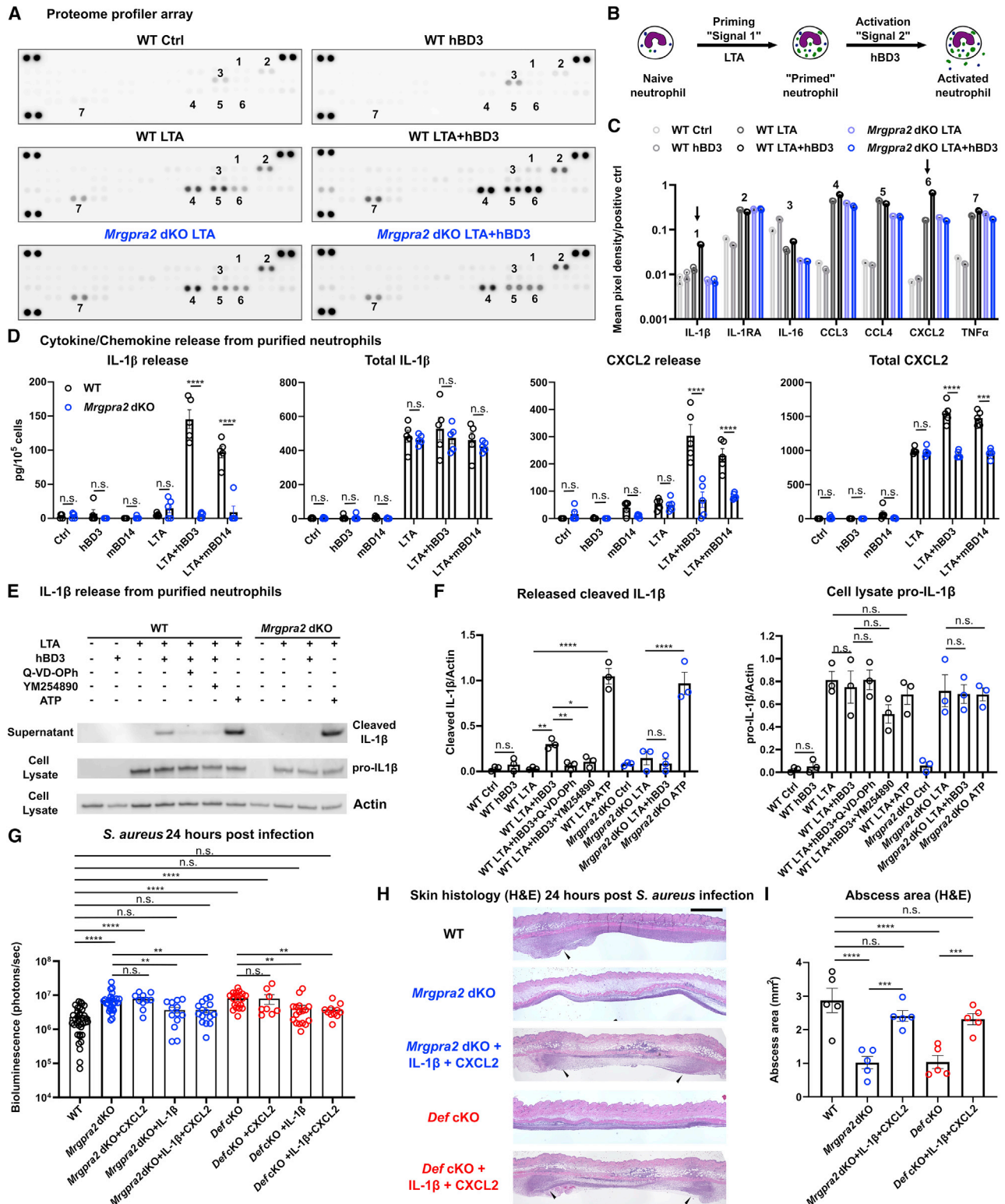


**Figure 7. Defensin-Mrgpra2 interaction triggered neutrophil release of IL-1β and CXCL2**

(A) Proteome profiler array analysis of culture medium of bone marrow neutrophils purified from WT (black) or *Mrgpra2* dKO (blue) animals stimulated by control medium, hBD3 only, *S. aureus* lipoteichoic acid (LTA), or LTA+hBD3. Numbers: 1, IL-1β; 2, IL-1RA; 3, IL-16; 4, CCL3; 5, CCL4; 6, CXCL2; 7, TNFα. Quantifications are shown in (C).

(B) Schematic illustration of experimental design. Neutrophils are first primed with LTA ("signal 1"), then activated by hBD3 ("signal 2").

(legend continued on next page)

neutrophils remains to be elucidated. Second, RNAscope showed that *Mrgpra2*<sup>+</sup> neutrophils accounted for about half of Ly6G<sup>+</sup> cells in the bone marrow. Recent single-cell analyses revealed heterogeneity and tissue specificities in neutrophil populations (Ballesteros et al., 2020; Xie et al., 2020). Detailed analyses using reporter mouse lines will be necessary for understanding important properties of the *Mrgpra2*<sup>+</sup> subpopulation, their development, trafficking, localization, and gene expression regulation in response to infections.

Our current study focused on the contribution of neutrophils to defensin-mediated innate immunity upon bacterial infection and skin microbiome homeostasis. However, it is likely that immune cells other than neutrophils contribute to defensin-evoked immunity and that other defensin receptors besides *Mrgpra2* function in these immune cells (Röhrl et al., 2010; Subramanian et al., 2013; Tseng and Hoon, 2022; Yang et al., 1999). Neutrophils do not exist in large numbers in the naive skin but are rapidly recruited from the blood stream following infections and inflammations (Hamid et al., 2021; Kolaczowska and Kubes, 2013). Tissue-resident immune cells including mast cells and macrophages are important for the initial phase of neutrophil recruitment before the neutrophil self-amplification loop reaches a critical mass (Arifuzzaman et al., 2019; De Filippo et al., 2008, 2013; Kim and Luster, 2015; Nestle et al., 2009; Pundir et al., 2019; Subramanian et al., 2013). Intra-vital imaging analyses can potentially be used to precisely quantify the roles of defensins and defensin receptors in regulating cellular dynamics following infections (Kolaczowska and Kubes, 2013). The defensin-neutrophil axis presented in this study added an important piece to the complex and intricate signaling networks at host-microbe interfaces (Kabashima et al., 2019).

The *Def* gene family is one of the largest gene families in the mouse genome. The exact reason for the organism to require these redundant peptides is unclear. Genetic analysis in *Drosophila* has revealed convincing functional diversities of AMPs (Hanson et al., 2019; Lazzaro et al., 2020). In the context of anti-*S. aureus* skin immunity, two mouse peptides mBD3 and mBD14 (and its human homolog hBD3) appeared to be of central importance. Among mouse defensins, mBD3 and mBD14 bear the largest number of positive charges (+10.6 and +11.6, respectively) and are the most potent in both their abilities to directly kill pathogens and activate immune receptors

(Midorikawa et al., 2003; Röhrl et al., 2008, 2010; Subramanian et al., 2013). The transcripts of *Defb3* and *Defb14* were among the most highly up-regulated after *S. aureus* infections. More intriguingly, in the absence of the entire *Def* gene cluster, supplying the human peptide hBD3 (homolog of mBD14) alone could restore the *S. aureus* infection phenotype to one similar to the WT animals. This suggested that despite the apparent genetic redundancy, a single potent peptide could be sufficient to restrict *S. aureus* infection. In the future, it would be interesting to dissect the roles of various AMPs, their relative importance in combating different classes of pathogens (including Gram positive and negative bacteria, viruses, and fungi), the types of host immune cells they activate and the receptors they employ. Another key question about AMPs that remains to be answered is the relative importance of direct killing versus immune-modulation. The strong loss-of-function phenotypes of the neutrophil receptors *Mrgpra2* supported the importance of innate immune cells in response to defensin signaling. However, given that defensins have been clearly shown to be capable of directly killing *S. aureus* (Harder et al., 2001; Hinrichsen et al., 2008; Midorikawa et al., 2003; Röhrl et al., 2008), both functions of these peptides are probably important in the host's ability to defeat the bacteria during infections. To definitively distinguish the relative contributions of direct killing versus immune modulation, stringent structure-function analyses will need to be performed to generate peptides lacking one aspect of their function while retaining the other. Ongoing efforts using cryogenic electron microscopy (cryo-EM) to illuminate the structure and ligand binding mechanisms of the MRGPR family receptors might provide an entry point to this difficult and important problem (Cao et al., 2021; Yang et al., 2021).

Last but not least, our finding has important implications in the pathologies of skin diseases. Studies of the skin microbiota have yielded important knowledge about the instructive roles that commensal microbiota play during the development of the host immune system and causal links between dysbiosis and inflammatory skin diseases (Grice et al., 2009; Liu et al., 2017; Naik et al., 2012, 2015; Nakatsuji et al., 2017; Wang et al., 2021; Williams and Gallo, 2017; Williams et al., 2017b). However, host factors defining the microenvironment for the microbiota remain largely unclear. Physical and chemical properties of the skin surface such as moisture and acidity have been known to

(C) Quantification of mean pixel intensity of proteome profiler arrays shown in (A). Arrows point to IL-1 $\beta$  (1 in A) and CXCL2 (6 in A), whose releases were enhanced by hBD3. Pixel intensities were normalized to positive controls on the same array.

(D) ELISA quantification of IL-1 $\beta$  and CXCL2 release from neutrophils. WT neutrophils pretreated with LTA released IL-1 $\beta$  and CXCL2 in response to hBD3 or mBD14 stimuli (black). Neutrophils purified from *Mrgpra2* dKO animals failed to respond to hBD3 (blue). Total IL-1 $\beta$  and CXCL2 was calculated as the sum of secreted and intracellular amounts. hBD3 or mBD14 alone did not induce the synthesis of IL-1 $\beta$  or CXCL2. n = 5.

(E) Western blot showing the release of mature IL-1 $\beta$  (17 kDa) released into the supernatant by WT neutrophils when stimulated with hBD3 (5  $\mu$ M). IL-1 $\beta$  release was inhibited by pan-caspase inhibitor Q-VD-OPH and G<sub>q</sub> inhibitor YM-254890 and was abolished in the *Mrgpra2* mutant neutrophils. ATP (5 mM) was used as positive control.

(F) Quantification of western blots of released IL-1 $\beta$  (17 kDa) and cellular pro-IL-1 $\beta$  (31 kDa) normalized to actin. n = 3.

(G) Bacteria bioluminescence 24 h post-*S. aureus* infection. CXCL2 alone did not rescue *Mrgpra2* or *Def* KO phenotypes, whereas IL-1 $\beta$  or IL-1 $\beta$ +CXCL2 together rescued the anti-*S. aureus* defect of *Mrgpra2* dKO and *Def* cKO mice. n = 8–36.

(H) H&E staining showing that injecting IL-1 $\beta$  and CXCL2 restored abscess formation in *Mrgpra2* dKO (blue) and *Def* cKO (red) animals 24 h post-*S. aureus* infection. Arrow heads point to neutrophil abscesses. Scale bar, 1 mm.

(I) Quantification of abscess areas based on H&E staining shown in (H). n = 5.

Results are presented as mean  $\pm$  SEM from at least three independent experiments. \*p < 0.05, \*\*p < 0.01, \*\*\*p < 0.001, \*\*\*\*p < 0.0001, n.s., not significant by one-way ANOVA.

See also Figure S7.

profoundly influence microbiome composition (Grice et al., 2009). However, influence from the host immune system, whose primary function is to interact with the microbial world, remains largely unknown. Defects in defensin production and neutrophil recruitment have been implicated in skin disease conditions involving severe microbiome dysbiosis (Chiang et al., 2019; Harder et al., 1997; Hollox et al., 2008). Here, we established a direct causal link between genetic deletion of the defensin-Mrgpra2 signaling pathway and skin dysbiosis. These findings suggest that normal skin maintains a baseline of immune activity and profoundly influences the microbiome composition on the surface (Matsumoto et al., 2021). Crosstalk between the epithelium and neutrophils through AMPs and their GPCRs are an important component of this baseline immune activity. Exactly how this system maintains a balanced microbiome, permitting colonization by commensal bacteria while restricting the expansion of pathogenic bacteria deserves further investigation. Overall, this study opens avenues to study innate immunity and could lead to improved therapies to treat infections and skin diseases related to AMP deregulation.

### Limitations of the study

Due to the large number of genes in the *Def* cluster and technical difficulty in peptide synthesis, we were unable to test every single defensin for its ability to activate *Mrgpra2* or regulate skin immunity. Although the *Def* cKO mouse is a powerful genetic tool to examine the collective loss-of-function consequences of defensins, it does not explain the diversity and specificity of this important AMP family. This study is limited to skin immunity, and it remains unknown whether other epithelial surfaces including the airway, intestines, and urogenital tracts employ similar epithelial-neutrophil axes to maintain healthy microbiota and fight infections.

### STAR★METHODS

Detailed methods are provided in the online version of this paper and include the following:

- KEY RESOURCES TABLE
- RESOURCE AVAILABILITY
  - Lead contact
  - Materials availability
  - Data and code availability
- EXPERIMENTAL MODEL AND SUBJECT DETAILS
  - Mice
  - Bacterial strains
- METHOD DETAILS
  - Generation of *Mrgpra2* dKO and *Def* cKO mice
  - Fluorescence-activated cell sorting (FACS) of innate immune cells
  - RNAscope® *in situ* hybridization
  - Calcium imaging
  - Co-IP
  - Western blot
  - $K_D$  determination by flow cytometry
  - Protein quantification by ELISA
  - 16S sequencing
  - Histology

- RNA extraction and quantification
- RNA sequencing
- Mouse models of *S. aureus* skin infection and quantification by IVIS
- Adoptive transfer of neutrophils
- Flow cytometry
- Isolation and stimulation of bone marrow neutrophils
- QUANTIFICATION AND STATISTICAL ANALYSIS

### SUPPLEMENTAL INFORMATION

Supplemental information can be found online at <https://doi.org/10.1016/j.immuni.2022.06.021>.

### ACKNOWLEDGMENTS

The authors thank Dr. Caiying Guo and the Janelia Farm Gene Targeting and Transgenics Team for generating the *Def<sup>fllox</sup>* mice, Chip Hawkins at the Johns Hopkins Transgenic Core for generating the *Mrgpra2* dKO mice, Christopher Blair at the University of Michigan Microbiome Core for 16S sequencing, Anuj Gupta at the Johns Hopkins SKCCC Experimental and Computational Genomics Core for 16S data analyses, and Dongeun Heo and the Johns Hopkins Transcriptomics and Deep Sequencing Core for RNA-seq. The work was supported by the Howard Hughes Medical Institute (Xinzhong Dong), a Damon Runyon Cancer Research Foundation Fellowship Award to Xintong Dong (DRG-2295-17), and NIH grants 1T32AR074920 and R01AR074846 to L.A.G., R01AI146177, R01AR073665, and R01AR069502 to N.K.A., R01AR070116, R01AR077007, and R21AI167047 to B.S.K., T32GM136577 to R.K. and C.V. and 2R37NS054791 to Xinzhong Dong. All work by L.M. was performed at prior affiliation, not present address.

### AUTHOR CONTRIBUTIONS

Xinzhong Dong, N.K.A., and Xintong Dong conceptualized and designed the study. Xintong Dong performed the experiments and analyzed the data under the supervision of Xinzhong Dong, L.S.M., and N.K.A. N.L. performed the EC<sub>50</sub> measurement of hBD3 on *Mrgpra2b*, Gram staining, anti-Ly6G antibody staining and FACS sorting and RT-PCR of *Mrgpra2* from immune cells. E.I.S. and M.L. designed and validated the *Mrgpra2* dKO mouse line. E.I.S. also designed and assisted with RNAscope *in situ* hybridization. This article was prepared while E.I.S. was employed at Johns Hopkins. The opinions expressed in this article are the author's own and do not reflect the view of the National Institutes of Health, the Department of Health and Human Services, or the United States government. G.W. assisted in the sample collection and data analysis of 16S sequencing under the supervision of L.A.G. R.V.O., D.D., and Y.W. assisted in *S. aureus* preparation and injection. C.Y. assisted with neutrophil purification and adoptive transfer. R.K. and C.V. designed and assisted with the biotin-hBD3-*Mrgpra2* binding experiments. M.P.A. provided expertise in inflammatory signaling and western blot. P.P. and B.S.K. contributed expertise in microbiology and dermatology. L.G. assisted in RNA-seq sample preparation. W.L. contributed expertise in defensin peptide structure and synthesis. Xintong Dong wrote the paper with input from all authors.

### DECLARATION OF INTERESTS

Xinzhong Dong is a co-founder and a scientific advisory board member of Escent Pharmaceuticals, a company focused on developing small molecules targeting MRGPRs. N.K.A. has received previous grant support from Pfizer and Boehringer Ingelheim and was a paid consultant for Janssen Pharmaceuticals. L.S.M. is currently a full-time paid employee of Janssen Research & Development, the pharmaceutical companies of Johnson & Johnson, and owns Johnson & Johnson stock. L.S.M. performed all work at his prior affiliation at Johns Hopkins University School of Medicine and he has received prior grant support from AstraZeneca, Pfizer, Boehringer Ingelheim, Regeneron Pharmaceuticals, and Moderna Therapeutics; was a paid consultant for Armirall and Janssen Research and Development; was on the scientific advisory board of Integrated Biotherapeutics; and is a shareholder of Noveome

Biotherapeutics, which are all developing therapeutics against infections (including *S. aureus* and other pathogens) and/or inflammatory conditions. B.S.K. has served as a consultant for AbbVie, ABRAX Japan, Almirall, Cara Therapeutics, Maruho, Menlo Therapeutics, Pfizer, and Third Rock Ventures. He has also participated on the advisory board for Almirall, Boehringer Ingelheim, Cara Therapeutics, Kiniksa Pharmaceuticals, Menlo Therapeutics, Regeneron Pharmaceuticals, Sanofi Genzyme, and Trevi Therapeutics. He is also Founder, Chief Scientific Officer, and stockholder of Nuogen Pharma, Inc. He is stockholder of Locus Biosciences. C.V. is a paid consultant and stockholder of AstraZeneca.

Received: July 6, 2021

Revised: April 19, 2022

Accepted: June 24, 2022

Published: July 25, 2022

## REFERENCES

- Abdul Hamid, A.I., Cara, A., Diot, A., Laurent, F., Josse, J., and Gueirard, P. (2021). Differential early in vivo dynamics and functionality of recruited polymorphonuclear neutrophils After infection by planktonic or biofilm *Staphylococcus aureus*. *Front. Microbiol.* *12*, 728429.
- Adolph, T.E., Tomczak, M.F., Niederreiter, L., Ko, H.J., Böck, J., Martinez-Naves, E., Glickman, J.N., Tschurtschenthaler, M., Hartwig, J., Hosomi, S., et al. (2013). Paneth cells as a site of origin for intestinal inflammation. *Nature* *503*, 272–276.
- Ahrens, K., Schunck, M., Podda, G.F., Meingassner, J., Stuetz, A., Schröder, J.M., Harder, J., and Proksch, E. (2011). Mechanical and metabolic injury to the skin barrier leads to increased expression of murine  $\beta$ -defensin-1, -3, and -14. *J. Invest. Dermatol.* *131*, 443–452.
- Ali, R.S., Falconer, A., Ikram, M., Bissett, C.E., Cerio, R., and Quinn, A.G. (2001). Expression of the peptide antibiotics human beta defensin-1 and human beta defensin-2 in normal human skin. *J. Invest. Dermatol.* *117*, 106–111.
- Amid, C., Rehaume, L.M., Brown, K.L., Gilbert, J.G.R., Dougan, G., Hancock, R.E.W., and Harrow, J.L. (2009). Manual annotation and analysis of the defensin gene cluster in the C57BL/6J mouse reference genome. *BMC Genomics* *10*, 606.
- Archer, N.K., Jo, J.H., Lee, S.K., Kim, D., Smith, B., Ortines, R.V., Wang, Y., Marchitto, M.C., Ravipati, A., Cai, S.S., et al. (2019). Injury, dysbiosis, and filaggrin deficiency drive skin inflammation through keratinocyte IL-1 $\alpha$  release. *J. Allergy Clin. Immunol.* *143*, 1426–1443.e6.
- Arifuzzaman, M., Mobley, Y.R., Choi, H.W., Bist, P., Salinas, C.A., Brown, Z.D., Chen, S.L., Staats, H.F., and Abraham, S.N. (2019). MRGPR-mediated activation of local mast cells clears cutaneous bacterial infection and protects against reinfection. *Sci. Adv.* *5*, eaav0216.
- Ballesteros, I., Rubio-Ponce, A., Genua, M., Lusito, E., Kwok, I., Fernández-Calvo, G., Khoiratty, T.E., van Grinsven, E., González-Hernández, S., Nicolás-Ávila, J.Á., et al. (2020). Co-option of neutrophil fates by tissue environments. *Cell* *183*, 1282–1297.e18.
- Bals, R., Wang, X., Meegalla, R.L., Wattler, S., Weiner, D.J., Nehls, M.C., and Wilson, J.M. (1999). Mouse  $\beta$ -defensin 3 is an inducible antimicrobial peptide expressed in the epithelia of multiple organs. *Infect. Immun.* *67*, 3542–3547.
- Bolyen, E., Rideout, J.R., Dillon, M.R., Bokulich, N.A., Abnet, C.C., Al-Ghalith, G.A., Alexander, H., Alm, E.J., Arumugam, M., Asnicar, F., et al. (2019). Reproducible, interactive, scalable and extensible microbiome data science using QIIME 2. *Nat. Biotechnol.* *37*, 852–857.
- Borregaard, N., Sørensen, O.E., and Theilgaard-Mönch, K. (2007). Neutrophil granules: a library of innate immunity proteins. *Trends Immunol.* *28*, 340–345.
- Byrd, A.L., Belkaid, Y., and Segre, J.A. (2018). The human skin microbiome. *Nat. Rev. Microbiol.* *16*, 143–155.
- Cao, C., Kang, H.J., Singh, I., Chen, H., Zhang, C., Ye, W., Hayes, B.W., Liu, J., Gumpfer, R.H., Bender, B.J., et al. (2021). Structure, function and pharmacology of human itch GPCRs. *Nature* *600*, 170–175.
- Cassatella, M.A., Östberg, N.K., Tamassia, N., and Soehnlein, O. (2019). Biological roles of neutrophil-derived granule proteins and cytokines. *Trends Immunol.* *40*, 648–664.
- Chen, Y.E., Fischbach, M.A., and Belkaid, Y. (2018). Skin microbiota-host interactions. *Nature* *553*, 427–436.
- Chessa, C., Bodet, C., Jousselin, C., Wehbe, M., Lévêque, N., and Garcia, M. (2020). Antiviral and immunomodulatory properties of antimicrobial peptides produced by human keratinocytes. *Front. Microbiol.* *11*, 1155.
- Chiang, C.C., Cheng, W.J., Korinek, M., Lin, C.Y., and Hwang, T.L. (2019). Neutrophils in psoriasis. *Front. Immunol.* *10*, 2376.
- Cho, J.S., Guo, Y., Ramos, R.I., Hebroni, F., Plaisier, S.B., Xuan, C., Granick, J.L., Matsushima, H., Takashima, A., Iwakura, Y., et al. (2012). Neutrophil-derived IL-1 $\beta$  is sufficient for abscess formation in immunity against *Staphylococcus aureus* in mice. *PLoS Pathog.* *8*, e1003047.
- Chou, R.C., Kim, N.D., Sadik, C.D., Seung, E., Lan, Y., Byrne, M.H., Haribabu, B., Iwakura, Y., and Luster, A.D. (2010). Lipid-cytokine-chemokine cascade drives neutrophil recruitment in a murine model of inflammatory arthritis. *Immunity* *33*, 266–278.
- Corbin, B.D., Seeley, E.H., Raab, A., Feldmann, J., Miller, M.R., Torres, V.J., Anderson, K.L., Dattilo, B.M., Dunman, P.M., Gerads, R., et al. (2008). Metal chelation and inhibition of bacterial growth in tissue abscesses. *Science* *319*, 962–965.
- Davis, S.E., Hopke, A., Minkin, S.C., Jr., Montedonico, A.E., Wheeler, R.T., and Reynolds, T.B. (2014). Masking of  $\beta(1-3)$ -glucan in the cell wall of *Candida albicans* from detection by innate immune cells depends on phosphatidylserine. *Infect. Immun.* *82*, 4405–4413.
- De Filippo, K., Dudeck, A., Hasenberg, M., Nye, E., van Rooijen, N., Hartmann, K., Gunzer, M., Roers, A., and Hogg, N. (2013). Mast cell and macrophage chemokines CXCL1/CXCL2 control the early stage of neutrophil recruitment during tissue inflammation. *Blood* *121*, 4930–4937.
- De Filippo, K., Henderson, R.B., Laschinger, M., and Hogg, N. (2008). Neutrophil chemokines KC and macrophage-inflammatory Protein-2 are newly synthesized by tissue macrophages using distinct TLR signaling pathways. *J. Immunol.* *180*, 4308–4315.
- Dillen, C.A., Pinsker, B.L., Marusina, A.I., Merleev, A.A., Farber, O.N., Liu, H., Archer, N.K., Lee, D.B., Wang, Y., Ortines, R.V., et al. (2018). Clonally expanded  $\gamma\delta$  T cells protect against *Staphylococcus aureus* skin reinfection. *J. Clin. Invest.* *128*, 1026–1042.
- Dwyer, D.F., Barrett, N.A., and Austen, K.F.; Immunological Genome Project Consortium (2016). Expression profiling of constitutive mast cells reveals a unique identity within the immune system. *Nat. Immunol.* *17*, 878–887.
- Eisenhauer, P.B., Harwig, S.S., and Lehrer, R.I. (1992). Cryptidins: antimicrobial defensins of the murine small intestine. *Infect. Immun.* *60*, 3556–3565.
- Ericson, J.A., Duffau, P., Yasuda, K., Ortiz-Lopez, A., Rothamel, K., Rifkin, I.R., and Monach, P.A.; ImmGen Consortium (2014). Gene expression during the generation and activation of mouse neutrophils: implication of novel functional and regulatory pathways. *PLoS One* *9*, e108553.
- Franchi, L., Kamada, N., Nakamura, Y., Burberry, A., Kuffa, P., Suzuki, S., Shaw, M.H., Kim, Y.G., and Núñez, G. (2012). NLRC4-driven production of IL-1 $\beta$  discriminates between pathogenic and commensal bacteria and promotes host intestinal defense. *Nat. Immunol.* *13*, 449–456.
- Gallo, R.L. (2017). Human skin is the largest epithelial surface for interaction with microbes. *J. Invest. Dermatol.* *137*, 1213–1214.
- Ganz, T. (2003). Defensins: antimicrobial peptides of innate immunity. *Nat. Rev. Immunol.* *3*, 710–720.
- Gerdol, M., Schmitt, P., Venier, P., Rocha, G., Rosa, R.D., and Destoumieux-Garzón, D. (2020). Functional insights From the evolutionary diversification of big defensins. *Front. Immunol.* *11*, 758.
- Grice, E.A., and Segre, J.A. (2011). The skin microbiome. *Nat. Rev. Microbiol.* *9*, 244–253.
- Grice, E.A., Kong, H.H., Conlan, S., Deming, C.B., Davis, J., Young, A.C., NISC Comparative Sequencing Program, Bouffard, G.G., Blakesley, R.W., Murray, P.R., et al. (2009). Topographical and temporal diversity of the human skin microbiome. *Science* *324*, 1190–1192.
- Guo, M., Cao, X., Zhang, K., Pan, M., Wu, Y., Langda, S., Yang, Y., Chen, Y., Gui, B., and Ma, B. (2022). 16S rRNA gene sequencing revealed changes in gut

- microbiota composition during pregnancy and lactation in mice model. *Vet. Sci.* **9**, 169.
- Hanson, M.A., Dostálová, A., Ceroni, C., Poidevin, M., Kondo, S., and Lemaitre, B. (2019). Synergy and remarkable specificity of antimicrobial peptides in vivo using a systematic knockout approach. *eLife* **8**, e44341.
- Harder, J., Bartels, J., Christophers, E., and Schröder, J.M. (1997). A peptide antibiotic from human skin. *Nature* **387**, 861.
- Harder, J., Bartels, J., Christophers, E., and Schroder, J.M. (2001). Isolation and characterization of human beta-defensin-3, a novel human inducible peptide antibiotic. *J. Biol. Chem.* **276**, 5707–5713.
- Hinrichsen, K., Podschun, R., Schubert, S., Schröder, J.M., Harder, J., and Proksch, E. (2008). Mouse beta-Defensin-14, an antimicrobial ortholog of human beta-Defensin-3. *Antimicrob. Agents Chemother.* **52**, 1876–1879.
- Hollox, E.J., Huffmeier, U., Zeeuwen, P.L.J.M., Palla, R., Lascorz, J., Rodijk-Olthuis, D., van de Kerkhof, P.C.M., Traupe, H., de Jongh, G., den Heijer, M., et al. (2008). Psoriasis is associated with increased beta-defensin genomic copy number. *Nat. Genet.* **40**, 23–25.
- Jiang, D., Saffarzadeh, M., and Scharffetter-Kochanek, K. (2017). In vitro demonstration and quantification of neutrophil extracellular trap formation. *Bio Protoc.* **7**, e2386.
- Kabashima, K., Honda, T., Ginhoux, F., and Egawa, G. (2019). The immunological anatomy of the skin. *Nat. Rev. Immunol.* **19**, 19–30.
- Kennedy, E.A., Connolly, J., ihane, J.O., Fallon, P.G., McLean, W.H.I., Murray, D., Jo, J.H., Segre, J.A., Kong, H.H., and Irvine, A.D. (2017). Skin microbiome before development of atopic dermatitis: early colonization with commensal staphylococci at 2 months is associated with a lower risk of atopic dermatitis at 1 year. *J. Allergy Clin. Immunol.* **139**, 166–172.
- Kim, N.D., and Luster, A.D. (2015). The role of tissue resident cells in neutrophil recruitment. *Trends Immunol.* **36**, 547–555.
- Kobayashi, S.D., Malachowa, N., and DeLeo, F.R. (2018). Neutrophils and bacterial immune evasion. *J. Innate Immun.* **10**, 432–441.
- Kobayashi, T., Glatz, M., Horiuchi, K., Kawasaki, H., Akiyama, H., Kaplan, D.H., Kong, H.H., Amagai, M., and Nagao, K. (2015). Dysbiosis and *Staphylococcus aureus* colonization drives inflammation in atopic dermatitis. *Immunity* **42**, 756–766.
- Kolaczowska, E., and Kubes, P. (2013). Neutrophil recruitment and function in health and inflammation. *Nat. Rev. Immunol.* **13**, 159–175.
- Kozich, J.J., Westcott, S.L., Baxter, N.T., Highlander, S.K., and Schloss, P.D. (2013). Development of a dual-index sequencing strategy and curation pipeline for analyzing amplicon sequence data on the MiSeq Illumina sequencing platform. *Appl. Environ. Microbiol.* **79**, 5112–5120.
- Krishna, S., and Miller, L.S. (2012). Host-pathogen interactions between the skin and *Staphylococcus aureus*. *Curr. Opin. Microbiol.* **15**, 28–35.
- Lämmermann, T., Afonso, P.V., Angermann, B.R., Wang, J.M., Kastenmüller, W., Parent, C.A., and Germain, R.N. (2013). Neutrophil swarms require LTB4 and integrins at sites of cell death in vivo. *Nature* **498**, 371–375.
- Lazzaro, B.P., Zasloff, M., and Rolf, J. (2020). Antimicrobial peptides: application informed by evolution. *Science* **368**, eaau5480.
- Lee, P.H.A., Ohtake, T., Zaiou, M., Murakami, M., Rudisill, J.A., Lin, K.H., and Gallo, R.L. (2005). Expression of an additional cathelicidin antimicrobial peptide protects against bacterial skin infection. *Proc. Natl. Acad. Sci. USA* **102**, 3750–3755.
- Lentini, G., Famà, A., Biondo, C., Mohammadi, N., Galbo, R., Mancuso, G., Iannello, D., Zummo, S., Giardina, M., De Gaetano, G.V., et al. (2020). Neutrophils enhance their own influx to sites of bacterial infection via endosomal TLR-dependent CXCL2 production. *J. Immunol.* **204**, 660–670.
- Ley, K., Laudanna, C., Cybulsky, M.I., and Nourshargh, S. (2007). Getting to the site of inflammation: the leukocyte adhesion cascade updated. *Nat. Rev. Immunol.* **7**, 678–689.
- Liu, H., Archer, N.K., Dillen, C.A., Wang, Y., Ashbaugh, A.G., Ortines, R.V., Kao, T., Lee, S.K., Cai, S.S., Miller, R.J., et al. (2017). *Staphylococcus aureus* epicutaneous exposure drives skin inflammation via IL-36-Mediated T cell responses. *Cell Host Microbe* **22**, 653–666.e5.
- Lone, A.G., Atci, E., Renslow, R., Beyenal, H., Noh, S., Fransson, B., Abu-Lail, N., Park, J.J., Gang, D.R., and Call, D.R. (2015). Colonization of Epidermal Tissue by *Staphylococcus aureus* Produces Localized Hypoxia and Stimulates Secretion of Antioxidant and caspase-14 Proteins. *Infect. Immun.* **83**, 3026–3034.
- Lotz, S., Aga, E., Wilde, I., van Zandbergen, G., Hartung, T., Solbach, W., and Laskay, T. (2004). Highly purified lipoteichoic acid activates neutrophil granulocytes and delays their spontaneous apoptosis via CD14 and TLR2. *J. Leukoc. Biol.* **75**, 467–477.
- Malhotra, N., Yoon, J., Leyva-Castillo, J.M., Galand, C., Archer, N., Miller, L.S., and Geha, R.S. (2016). IL-22 derived from  $\gamma\delta$  T cells restricts *Staphylococcus aureus* infection of mechanically injured skin. *J. Allergy Clin. Immunol.* **138**, 1098–1107.e3.
- Martinon, F., Burns, K., and Tschopp, J. (2002). The inflammasome: A molecular platform triggering activation of inflammatory caspases and processing of proIL-1 $\beta$ . *Mol. Cell* **10**, 417–426.
- Matsumoto, M., Nakagawa, S., Zhang, L., Nakamura, Y., Villaruz, A.E., Otto, M., Wolz, C., Inohara, N., and Núñez, G. (2021). Interaction between *Staphylococcus* Agr virulence and neutrophils regulates pathogen expansion in the skin. *Cell Host Microbe* **29**, 930–940.e4.
- Mayadas, T.N., Cullere, X., and Lowell, C.A. (2014). The multifaceted functions of neutrophils. *Annu. Rev. Pathol.* **9**, 181–218.
- McNeil, B.D., Pundir, P., Meeker, S., Han, L., Udem, B.J., Kulka, M., and Dong, X. (2015). Identification of a mast-cell-specific receptor crucial for pseudo-allergic drug reactions. *Nature* **519**, 237–241.
- Meylan, P., Lang, C., Mermoud, S., Johannsen, A., Norrenberg, S., Hohl, D., Vial, Y., Prod'Hom, G., Greub, G., Kyriiotou, M., et al. (2017). Skin colonization by *Staphylococcus aureus* precedes the clinical diagnosis of atopic dermatitis in infancy. *J. Invest. Dermatol.* **137**, 2497–2504.
- Midorikawa, K., Ouhara, K., Komatsuzawa, H., Kawai, T., Yamada, S., Fujiwara, T., Yamazaki, K., Sayama, K., Taubman, M.A., Kurihara, H., et al. (2003). *Staphylococcus aureus* susceptibility to innate antimicrobial peptides, beta-defensins and CAP18, expressed by human keratinocytes. *Infect. Immun.* **71**, 3730–3739.
- Miller, L.S., and Cho, J.S. (2011). Immunity against *Staphylococcus aureus* cutaneous infections. *Nat. Rev. Immunol.* **11**, 505–518.
- Miller, L.S., O'Connell, R.M., Gutierrez, M.A., Pietras, E.M., Shahangian, A., Gross, C.E., Thirumala, A., Cheung, A.L., Cheng, G., and Modlin, R.L. (2006). MyD88 mediates neutrophil recruitment initiated by IL-1R but not TLR2 activation in immunity against *Staphylococcus aureus*. *Immunity* **24**, 79–91.
- Miller, L.S., Pietras, E.M., Uricchio, L.H., Hirano, K., Rao, S., Lin, H., O'Connell, R.M., Iwakura, Y., Cheung, A.L., Cheng, G., et al. (2007). Inflammasome-mediated production of IL-1 $\beta$  is required for neutrophil recruitment against *Staphylococcus aureus* in vivo. *J. Immunol.* **179**, 6933–6942.
- Miranda, I., Uriarte, S.M., and McLeish, K.R. (2017). Multiple phenotypic changes define neutrophil priming. *Front. Cell. Infect. Microbiol.* **7**, 217.
- Molloy, M.J., Grainger, J.R., Bouladoux, N., Hand, T.W., Koo, L.Y., Naik, S., Quinones, M., Dzutsev, A.K., Gao, J.L., Trinchieri, G., et al. (2013). Intraluminal containment of commensal outgrowth in the gut during infection-induced dysbiosis. *Cell Host Microbe* **14**, 318–328.
- Morrison, G., Kilanowski, F., Davidson, D., and Dorin, J. (2002). Characterization of the mouse beta defensin 1, Defb1, mutant mouse model. *Infect. Immun.* **70**, 3053–3060.
- Naik, S., Bouladoux, N., Linehan, J.L., Han, S.J., Harrison, O.J., Wilhelm, C., Conlan, S., Himmelfarb, S., Byrd, A.L., Deming, C., et al. (2015). Commensal-dendritic-cell interaction specifies a unique protective skin immune signature. *Nature* **520**, 104–108.
- Naik, S., Bouladoux, N., Wilhelm, C., Molloy, M.J., Salcedo, R., Kastenmuller, W., Deming, C., Quinones, M., Koo, L., Conlan, S., et al. (2012). Compartmentalized control of skin immunity by resident commensals. *Science* **337**, 1115–1119.

- Nakatsuji, T., Chen, T.H., Narala, S., Chun, K.A., Two, A.M., Yun, T., Shafiq, F., Kotel, P.F., Bouslimani, A., Melnik, A.V., et al. (2017). Antimicrobials from human skin commensal bacteria protect against *Staphylococcus aureus* and are deficient in atopic dermatitis. *Sci. Transl. Med.* **9**, eaah4680.
- Nakatsuji, T., and Gallo, R.L. (2012). Antimicrobial peptides: old molecules with new ideas. *J. Invest. Dermatol.* **132**, 887–895.
- Navid, F., Boniotto, M., Walker, C., Ahrens, K., Proksch, E., Sparwasser, T., Müller, W., Schwarz, T., and Schwarz, A. (2012). Induction of regulatory T cells by a murine  $\beta$ -defensin. *J. Immunol.* **188**, 735–743.
- Nestle, F.O., Di Meglio, P., Qin, J.Z., and Nickoloff, B.J. (2009). Skin immune sentinels in health and disease. *Nat. Rev. Immunol.* **9**, 679–691.
- Pasparakis, M., Haase, I., and Nestle, F.O. (2014). Mechanisms regulating skin immunity and inflammation. *Nat. Rev. Immunol.* **14**, 289–301.
- Pundir, P., Liu, R., Vasavda, C., Serhan, N., Limjunyawong, N., Yee, R., Zhan, Y., Dong, X., Wu, X., Zhang, Y., et al. (2019). A connective tissue mast-cell-specific receptor detects bacterial quorum-sensing molecules and mediates antibacterial immunity. *Cell Host Microbe* **26**, 114–122.e8.
- Ridder, M.J., McReynolds, A.K.G., Dai, H., Pritchard, M.T., Markiewicz, M.A., and Bose, J.L. (2022). Kinetic characterization of the immune response to methicillin-resistant *Staphylococcus aureus* subcutaneous skin infection. *Infect. Immun.* e0006522.
- Röhrl, J., Yang, D., Oppenheim, J.J., and Hehlgans, T. (2008). Identification and Biological Characterization of Mouse beta-defensin 14, the orthologue of human beta-defensin 3. *J. Biol. Chem.* **283**, 5414–5419.
- Röhrl, J., Yang, D., Oppenheim, J.J., and Hehlgans, T. (2010). Human beta-defensin 2 and 3 and their mouse orthologs induce chemotaxis through interaction with CCR2. *J. Immunol.* **184**, 6688–6694.
- Sadik, C.D., Kim, N.D., and Luster, A.D. (2011). Neutrophils cascading their way to inflammation. *Trends Immunol.* **32**, 452–460.
- Salzman, N.H., Ghosh, D., Huttner, K.M., Paterson, Y., and Bevins, C.L. (2003). Protection against enteric salmonellosis in transgenic mice expressing a human intestinal defensin. *Nature* **422**, 522–526.
- Shi, J., Zhao, Y., Wang, K., Shi, X., Wang, Y., Huang, H., Zhuang, Y., Cai, T., Wang, F., and Shao, F. (2015). Cleavage of GSDMD by inflammatory caspases determines pyroptotic cell death. *Nature* **526**, 660–665.
- Sievers, F., Wilm, A., Dineen, D., Gibson, T.J., Karplus, K., Li, W., Lopez, R., McWilliam, H., Remmert, M., Söding, J., et al. (2011). Fast, scalable generation of high-quality protein multiple sequence alignments using Clustal Omega. *Mol. Syst. Biol.* **7**, 539.
- Singh, G., Inoue, A., Gutkind, J.S., Russell, R.B., and Raimondi, F. (2019). PRECOG: PREdicting COupling probabilities of G-protein coupled receptors. *Nucleic Acids Res.* **47**, W395–W401.
- Subramanian, H., Gupta, K., Lee, D., Bayir, A.K., Ahn, H., and Ali, H. (2013).  $\beta$ -Defensins activate human mast cells via Mas-related gene X2. *J. Immunol.* **191**, 345–352.
- Sumikawa, Y., Asada, H., Hoshino, K., Azukizawa, H., Katayama, I., Akira, S., and Itami, S. (2006). Induction of beta-defensin 3 in keratinocytes stimulated by bacterial lipopeptides through toll-like receptor 2. *Microbes Infect.* **8**, 1513–1521.
- Tkaczyk, C., Hamilton, M.M., Datta, V., Yang, X.P., Hilliard, J.J., Stephens, G.L., Sadowska, A., Hua, L., O'Day, T., Suzich, J., et al. (2013). *Staphylococcus aureus* Alpha toxin suppresses effective innate and adaptive immune responses in a murine dermonecrosis model. *PLoS One* **8**, e75103.
- Tseng, P.Y., and Hoon, M.A. (2022). Specific  $\beta$ -defensins stimulate pruritus through activation of sensory neurons. *J. Invest. Dermatol.* **142**, 594–602.
- Uhlen, M., Karlsson, M.J., Zhong, W., Tebani, A., Pou, C., Mikes, J., Lakshmikanth, T., Forsström, B., Edfors, F., Odeberg, J., et al. (2019). A genome-wide transcriptomic analysis of protein-coding genes in human blood cells. *Science* **366**, eaax9198.
- Wang, G., Sweren, E., Liu, H., Wier, E., Alphonse, M.P., Chen, R., Islam, N., Li, A., Xue, Y., Chen, J., et al. (2021). Bacteria induce skin regeneration via IL-1 $\beta$  signaling. *Cell Host Microbe* **29**, 777–791.e6.
- Williams, H., Crompton, R.A., Thomason, H.A., Campbell, L., Singh, G., McBain, A.J., Cruickshank, S.M., and Hardman, M.J. (2017a). Cutaneous Nod2 Expression Regulates the Skin microbiome and Wound Healing in a Murine Model. *J. Invest. Dermatol.* **137**, 2427–2436.
- Williams, M.R., and Gallo, R.L. (2017). Evidence that human skin microbiome dysbiosis promotes atopic dermatitis. *J. Invest. Dermatol.* **137**, 2460–2461.
- Williams, M.R., Nakatsuji, T., and Gallo, R.L. (2017b). *Staphylococcus aureus*: Master Manipulator of the Skin. *Cell Host Microbe* **22**, 579–581.
- Wilson, C.L., Ouellette, A.J., Satchell, D.P., Ayabe, T., López-Boado, Y.S., Stratman, J.L., Hultgren, S.J., Matrisian, L.M., and Parks, W.C. (1999). Regulation of intestinal alpha-defensin activation by the metalloproteinase matrilysin in innate host defense. *Science* **286**, 113–117.
- Wright, H.L., Thomas, H.B., Moots, R.J., and Edwards, S.W. (2013). RNA-seq reveals activation of both common and cytokine-specific pathways following neutrophil priming. *PLoS One* **8**, e58598.
- Xie, X., Shi, Q., Wu, P., Zhang, X., Kambara, H., Su, J., Yu, H., Park, S.Y., Guo, R., Ren, Q., et al. (2020). Single-cell transcriptome profiling reveals neutrophil heterogeneity in homeostasis and infection. *Nat. Immunol.* **21**, 1119–1133.
- Yang, D., Chertov, O., Bykovskaia, S.N., Chen, Q., Buffo, M.J., Shogan, J., Anderson, M., Schröder, J.M., Wang, J.M., Howard, O.M., et al. (1999). Beta-defensins: linking innate and adaptive immunity through dendritic and T cell CCR6. *Science* **286**, 525–528.
- Yang, D., Han, Z., and Oppenheim, J.J. (2017). Alarmins and immunity. *Immunol. Rev.* **280**, 41–56.
- Yang, F., Guo, L., Li, Y., Wang, G., Wang, J., Zhang, C., Fang, G.X., Chen, X., Liu, L., Yan, X., et al. (2021). Structure, function and pharmacology of human itch receptor complexes. *Nature* **600**, 164–169.
- Zambrano, S., Möller-Hackbarth, K., Li, X., Rodriguez, P.Q., Charrin, E., Schwarz, A., Nyström, J., Wernerson, A.O., Lal, M., and Patrakka, J. (2019). GPRC5b Modulates Inflammatory Response in Glomerular Diseases via NF- $\kappa$ B Pathway. *J Am Soc Nephrol.* **30**, 1573–1586.
- Zhao, Y., Yang, S., Li, B., Li, W., Wang, J., Chen, Z., Yang, J., Tan, H., and Li, J. (2019). Alterations of the mice gut microbiome via *Schistosoma japonicum* ova-induced granuloma. *Front. Microbiol.* **10**, 352.
- Zhou, Y.S., Webb, S., Lettice, L., Tardif, S., Kilanowski, F., Tyrrell, C., MacPherson, H., Semple, F., Tennant, P., Baker, T., et al. (2013). Partial Deletion of chromosome 8  $\beta$ -defensin Cluster Confers Sperm Dysfunction and Infertility in Male Mice. *PLoS Genet.* **9**, e1003826.

STAR★METHODS

KEY RESOURCES TABLE

REAGENT or RESOURCE	SOURCE	IDENTIFIER
<b>Antibodies</b>		
Anti-biotin PE clone 1D4-C5	Biolegend	Cat# 409004; RRID: AB_10641847
Anti-biotin	Abcam	Cat# ab53494; RRID: AB_867860
Sepharose anti-GFP antibody	Abcam	Cat# ab69314; RRID: AB_1640178
Anti-GFP	Thermo Fisher	Cat# A-11122; RRID: AB_221569
Anti-rabbit IgG HRP-conjugated	R&D systems	Cat# HAF008; RRID: AB_357235
Rat monoclonal anti-mouse Ly6G clone 1A8	BioXCell	Cat# BE0075-1; RRID: AB_1107721
Rat monoclonal IgG2a isotype control clone 2A3	BioXCell	Cat# BE0089; RRID: AB_1107769
Anti-mouse CD45 APC-Cy7 clone 30-F11	Biolegend	Cat# 103116; RRID: AB_312981
Anti-mouse CD11b PE/Dazzle594 Clone M1/70	Biolegend	Cat# 101256; RRID: AB_2563648
Anti-mouse CD11c PE/Cy7 Clone N418	Biolegend	Cat# 117318; RRID: AB_493568
Anti-mouse Ly6C APC Clone HK1.4	Biolegend	Cat# 128016; RRID: AB_1732076
Anti-mouse Ly6G BV421 Clone 1A8	Biolegend	Cat# 127628; RRID: AB_2562567
Anti-mouse F4/80 BV605 Clone BM8	Biolegend	Cat# 123133; RRID: AB_2562305
Anti-mouse Siglec F BB515 Clone E50-2440	BD Bioscience	Cat# 564514; RRID: AB_2738833
Anti-mouse c-Kit BV421 Clone ACK2	Biolegend	Cat# 135124; RRID: AB_2562237
Anti-mouse ICAM FITC Clone YN/1.7.4	Biolegend	Cat# 116105; RRID: AB_313696
Anti-mouse F4/80 PE Clone BM8	Biolegend	Cat# 123110; RRID: AB_893486
Anti-mouse FcεRI PE/Cy7 Clone MAR-1	Biolegend	Cat# 134318; RRID: AB_10640122
Anti-mouse CD11b BV785 Clone M1/70	Biolegend	Cat# 101243; RRID: AB_2561373
Anti-mouse CD11c BV605 Clone N418	Biolegend	Cat# 117334; RRID: AB_2562415
Anti-mouse I-A/I-E BV711 Clone M5/114.15.2	Biolegend	Cat# 107643; RRID: AB_2565976
Anti-mouse Ly6G PE/Cy7 Clone 1A8	Biolegend	Cat# 127617; RRID: AB_1877262
Anti-mouse CD11b PE Clone M1/70	Biolegend	Cat# 101207; RRID: AB_312790
Anti-mouse B220 APC Clone RA3-6B2	eBioscience	Cat# 17-0452-82; RRID: AB_469395
Anti-mouse Ly6G AF700 Clone 1A8	Biolegend	Cat# 127622; RRID: AB_10643269
Anti-mouse CD49b PE Clone DX5	Biolegend	Cat# 108908; RRID: AB_313415
Rabbit anti-mouse BD14	MyBioSource	Cat# MBS1490249; RRID: AB_2732866
Rat anti-mouse Ly6G	Biolegend	Cat# 127602; RRID: AB_1089180
Rabbit anti-S. Aureus	Abcam	Cat# 20920; RRID: AB_445913
Alexa Fluor® 488 goat anti-rabbit IgG	Thermo Fisher	Cat# A-11008; RRID: AB_143165
Alexa Fluor® 488 goat anti-rat IgG	Thermo Fisher	Cat# A-11006; RRID: AB_2534074
Alexa Fluor® 594 goat anti-rabbit IgG	Thermo Fisher	Cat# A-11012; RRID: AB_2534079
Goat anti-mouse IL-1β	R&D systems	Cat# AF-401-NA; RRID: AB_416684
Rabbit anti-cleaved-IL-1β	Cell Signaling Technology	Cat# 63124s
Rabbit anti-goat IgG HRP-conjugated	R&D systems	Cat# HAF017; RRID: AB_562588
HRP anti-beta Actin	Abcam	Cat# Ab49900; RRID: AB_867494
<b>Bacterial and virus strains</b>		
<i>Staphylococcus aureus</i> SF8300	Binh Diep (UCSF)	N/A
<i>Staphylococcus aureus</i> USA300 LAC::lux	Tammy Kielian (University of Nebraska)	N/A
<b>Chemicals, peptides, and recombinant proteins</b>		
hBD3	Anaspec	Cat# AS-60741
Biotin-hBD3	Anaspec	N/A

(Continued on next page)

**Continued**

REAGENT or RESOURCE	SOURCE	IDENTIFIER
mBD14	Wuyuan Lu (University of Maryland Baltimore)	N/A
mBD3	Wuyuan Lu (University of Maryland Baltimore)	N/A
<i>S. aureus</i> derived LTA	Invivogen	Cat# Tlrl-pslta
Tryptic soy broth	Millipore	Cat# 22092
TRIZOL reagent	Thermo Fisher	Cat# 15596018
Liberase TL	Roche	Cat# 05401054001
DNase I	Sigma-Aldrich	Cat# 4536282001
Recombinant mouse IL-1 $\beta$	R&D systems	Cat# 401-ML
Recombinant mouse CXCL2	R&D systems	Cat# 452-M2-050/CF
NuPAGE™ LDS Sample Buffer	Thermo Fisher	Cat# NP0007
Q-VD-Oph	R&D systems	Cat# OPH001-01M
YM254890	Tocris	Cat# 7352
SYTOX blue	Thermo Fisher	Cat# S34857
SYTOX red	Thermo Fisher	Cat# S34859
SYTOX orange	Thermo Fisher	Cat# S11368
<b>Critical commercial assays</b>		
Mouse Elastase DuoSet ELISA Kit	R&D systems	Cat# DY4517-05
Mouse MPO DuoSet ELISA Kit	R&D systems	Cat# DY3667
Mouse S100A8/A9 DuoSet ELISA Kit	R&D systems	Cat# DY8596-05
Mouse IL-1 $\beta$ DuoSet ELISA Kit	R&D systems	Cat# DY401-05
Mouse CXCL2 DuoSet ELISA Kit	R&D systems	Cat# DY452-05
Mouse BD14 ELISA Kit	MyBioSource	Cat# MBS2515829
MACS neutrophil isolation kit	Miltenyi Biotec	Cat# 130-097-658
RNAscope® Multiplex Fluorescent Detection Kit v2	ACDBio	Cat# 323110
RNAscope® <i>Ly6g</i> probe	ACDBio	Cat# 455701
RNAscope® <i>Mrgpra2</i> probe	ACDBio	Custom-made
RNeasy Plus Mini kit	Qiagen	Cat# 74034
Chemotaxis assay kit	Abcam	Cat# Ab235692
Cellular reactive oxygen species detection assay kit	Abcam	Cat# Ab113851
<b>Deposited data</b>		
RNA-seq data	NCBI GEO	GEO: GSE178507
<b>Experimental models: Cell lines</b>		
G $\alpha$ 15 HEK 293 cells	This study	N/A
Mrgpra2b-GFP; G $\alpha$ 15 HEK 293 cells	This study	N/A
MRGPRX3-FLAG; G $\alpha$ 15 HEK 293 cells	This study	N/A
MRGPRX4-GFP; G $\alpha$ 15 HEK 293 cells	This study	N/A
<b>Experimental models: Mice</b>		
C57BL/6J	Jackson laboratory	Cat# 000664
<i>Mrgpra2</i> dKO	This study	N/A
<i>K14-cre</i> ; <i>Def<sup>fllox/fllox</sup></i>	This study	N/A
<i>K14-cre</i>	Jackson laboratory	Cat# 018964

(Continued on next page)

REAGENT or RESOURCE	SOURCE	IDENTIFIER
<b>Continued</b>		
<b>Oligonucleotides</b>		
gRNAs targeting <i>Mrgpra2a/b</i> CAAGTTAGTTTTGGTCAATC, GATCTGATACCCTCTTCTGG, TAAACTGGCTATCTACTTGA, TTATCCAATGCTGGGATAAT	This study	N/A
Genotyping primers for <i>Mrgpra2</i> dKO GTCAGCATGATGGTCAC (WT-F), CATAGGGAAGGCCTCATGTCTC (WT-R), CTATGGAGGGATGCTCA TACTG ( <i>Mrgpra2</i> dKO-F), CAAGA TCTGACTCCCTCTTCTGG ( <i>Mrgpra2</i> dKO-R)	This study	N/A
gRNA targeting <i>Defb13</i> CCAAGCCAATTTCTGTGCTGCA	This study	N/A
gRNA targeting <i>Defb40</i> CCATGGGCATTTCTGAATGTGAC	This study	N/A
Primers for genotyping <i>Def</i> cluster deletion GATGCAGGTGCCCTGAAATAT (F) CACTGAATAGACCTGACTTCC (R)	This study	N/A
RT-PCR primer for <i>Mrgpra2</i> CCTCCTACACAAGCCAGCAA (F) AAGCACAAAGTAAAAGATGATGCT	This study	N/A
RT-PCR primer for <i>Gapdh</i> TGTTCTACCCCAATGTGT (F) TGTGAGGGAGATGCTCAGTG (R)	(Zambrano et al., 2019)	N/A
<b>Software and algorithms</b>		
FlowJo	BD	<a href="https://www.flowjo.com/">https://www.flowjo.com/</a>
GraphPad Prism 9	GraphPad	<a href="https://www.graphpad.com/scientific-software/prism/">https://www.graphpad.com/scientific-software/prism/</a>
ImageJ	NIH	<a href="https://fiji.sc/">https://fiji.sc/</a>
R	R	<a href="https://www.r-project.org/">https://www.r-project.org/</a>
QIIME2	QIIME2 development team	<a href="https://qiime2.org/">https://qiime2.org/</a>
STAR - 2.7.3a	Alexander Dobin	<a href="https://github.com/alexdobin/STAR/releases/tag/2.7.9a">https://github.com/alexdobin/STAR/releases/tag/2.7.9a</a>
Partek Flow	Partek	<a href="https://www.partek.com/">https://www.partek.com/</a>
Partek GS v7.0	Partek	<a href="https://www.partek.com/">https://www.partek.com/</a>
Spotfire	TIBCO	<a href="https://www.tibco.com/products/tibco-spotfire">https://www.tibco.com/products/tibco-spotfire</a>

## RESOURCE AVAILABILITY

### Lead contact

Further information and requests for resources and reagents should be directed to and will be fulfilled by the lead contact, Xinzhong Dong ([xdong2@jhmi.edu](mailto:xdong2@jhmi.edu)).

### Materials availability

Reagent and materials generated in this study are available from the lead contact without restriction.

### Data and code availability

- RNA-seq data have been deposited at Gene Expression Omnibus (GEO) and are publicly available as of the date of publication. Accession number is listed in the [key resources table](#).
- All data supporting the findings of this study are available in the manuscript or the [supplemental information](#) and are available upon request to the [lead contact](#) author.
- This paper does not report original code.
- Any additional information required to reanalyze the data reported in this paper is available from the [lead contact](#) upon request.

## EXPERIMENTAL MODEL AND SUBJECT DETAILS

### Mice

All experiments were performed in accordance with protocols approved by the Animal Care and Use Committee at the Johns Hopkins University School of Medicine. 8–10 weeks old, age- and gender-matched male and female mice on the C57BL/6J background were used for experiments. Detailed procedures for the generation of *Mrgpra2* dKO and *Def* cKO mouse lines are described in the [method details](#) section. For the 16S sequencing experiment, WT and mutant littermates were weaned by genotypes at three weeks old then housed with animals of the same genotype for six weeks under conventional housing conditions in a non-helico-bacter-free facility. Co-housed animals were used in all infection studies.

### Bacterial strains

Bioluminescent *S. aureus* SF8300 strain was used for epicutaneous *S. aureus* exposure ([Figure S4](#)). Bioluminescent USA300 LAC::*lux* strain was used in the intradermal injection model ([Figures 4, 5, 6, and 7](#)). Bacteria were streaked onto blood tryptic soy agar (TSA) plates (Thermo Fisher Scientific) and grown overnight at 37°C. Single colonies were picked and cultured in tryptic soy broth (TSB, Sigma) at 37°C in a shaking incubator (240 rpm) overnight, followed by a 1:50 subculture at 37°C for 2 hr to obtain mid-logarithmic phase bacteria. The bacteria were pelleted by centrifugation at 5000g, washed 3 times, and resuspended in sterile PBS to the required concentration. OD600 was taken to measure bacterial density. SF8300 was resuspended at 10<sup>9</sup> CFU/50μL per mouse. USA300 LAC::*lux* was resuspended at 3×10<sup>7</sup>/100μL per mouse.

## METHOD DETAILS

### Generation of *Mrgpra2* dKO and *Def* cKO mice

Sequences for all guide RNAs (gRNAs) and genotyping primers are listed in the [key resources table](#). *Mrgpra2* double knockout (dKO) animals were generated by the Johns Hopkins University School of Medicine Transgenic Core Laboratory using standard CRISPR/cas9 methods. gRNAs were designed to target the 5' untranslated regions (UTR) of *Mrgpra2a* and 3' UTR of *Mrgpra2b* and resulted in deletion of the entire genomic region including all exons of both *Mrgpra2a* and *Mrgpra2b*. *Def*<sup>fllox</sup> mice were generated by the Howard Hughes Medical Institute Janelia Research Campus Gene Targeting and Transgenics team using standard CRISPR/cas9 technique. The first *loxP* cassette was inserted in exon2 of *Defb13* by co-injecting Cas9 mRNA, gRNA and a repair template with *loxP* site flanked by 30 base pairs homology arms on each side. Animals bred homozygous for this *Defb13 loxP* allele were then mutated with another CRISPR construct targeting exon2 of *Defb40* and a second *loxP* repair template. The resulting *Def*<sup>fllox</sup> mice were then crossed with *K14-cre* mice to generate *K14-cre; Def*<sup>fllox/fllox</sup> conditional knock out (cKO) mice. PCR genotyping and Sanger sequencing were performed to confirm successful deletion of the entire cluster.

### Fluorescence-activated cell sorting (FACS) of innate immune cells

Dendritic cells were isolated from spleen; mast cells and macrophages were isolated from peritoneal lavage; neutrophils and basophils were isolated from bone marrow; and monocytes and eosinophils were isolated from peripheral blood. Single-cell suspensions from each tissue were subjected to red blood cell lysis using a hypotonic ammonium chloride-potassium (ACK) buffer (Quality Biological). Then, samples were incubated with CD16/CD32 Fc Blocker (Biolegend) for 10 min in FACS buffer (PBS supplemented with 2% fetal bovine serum). Surface staining was performed for 30 min at 4°C with the antibodies listed in [Table S1](#). Dead cells were stained with either SYTOX Blue or SYTOX Red (Thermo Fisher). Cell sorting was performed on the SONY SH800 cell sorter (Sony Biotechnology) with a 100 μm nozzle. Neutrophils were gated as SiglecF<sup>+</sup>Ly6G<sup>+</sup>CD11b<sup>+</sup>CD49b<sup>+</sup>SSC<sup>int</sup>; mast cells were gated as c-Kit<sup>+</sup>FcεRI<sup>+</sup>F4/80<sup>+</sup>ICAM<sup>-</sup>; basophils were gated as SiglecF<sup>+</sup>CD49b<sup>+</sup>FcεRI<sup>+</sup>c-Kit<sup>-</sup>SSC<sup>low</sup>; eosinophils were gated as SiglecF<sup>+</sup>Ly6G<sup>-</sup>CD11b<sup>-</sup>SSC<sup>high</sup>; monocytes were gated as TCRβ<sup>-</sup>B220<sup>-</sup>CD11b<sup>+</sup>Ly6G<sup>-</sup>SSC<sup>med</sup>; macrophages were gated as Ly6G<sup>-</sup>CD11b<sup>high</sup>F4/80<sup>high</sup>ICAM<sup>+</sup>; dendritic cells were gated as B220<sup>-</sup>CD11c<sup>high</sup>MHC-II<sup>+</sup>Ly6G<sup>-</sup>.

### RNAscope® *in situ* hybridization

Bone marrow was collected from the femur and tibia bones of WT and *Mrgpra2* dKO mice. Red blood cells were lysed in ACK lysing buffer (Quality Biological). Remaining cells were cytopun onto poly-L-lysine-coated glass slides (Fisher Scientific) and fixed in 10% neutral buffered formalin. Slides were washed in PBS for 5 min and treated with protease for 15 min at 40°C. Target probes for *Ly6g* and *Mrgpra2b* were combined and hybridized for 2 hours at 4°C using the HybEZ Hybridization System. Following amplification and label application according to manufacturer instructions, slides were imaged with a Zeiss LSM700 confocal microscope.

### Calcium imaging

HEK293 cells stably expressing a Gα15 subunit were transfected with constructs containing the cDNA of *Mrgpra2b*, MRGPRX3 or MRGPRX4. Mock-transfected cells were used as controls. Cells were plated onto 96 well plates and grown to 80–90% confluence, then incubated at 37°C with the FLIPR Calcium 5 calcium indicator (Molecular Devices) in Hank's Balanced Salt Solution (HBSS, Millipore Sigma) with 20 mM HEPES (ThermoFisher) for 1 hour, equilibrated at room temperature for 15 min and imaged on Flex Station 3 (Molecular Devices). Baseline was recorded for 20 sec, peptides were added, and intracellular Ca<sup>2+</sup> response was recorded for 150 sec. 2–9 duplicate experiments were averaged and EC<sub>50</sub> values were determined by normalizing to the peak response.

### Co-IP

HEK cells expressing Mrgpra2b-GFP or MRGPRX4-GFP (negative control) were cultured to confluence in T75 flasks and lysed in co-IP lysis buffer (50mM Tris HCl, pH=7.4, 150 mM NaCl, 1% Triton X-100, 5% Glycerol) at  $10^7$  cells/mL. 1 mL of cell lysates were incubated with sepharose anti-GFP beads (Abcam) and 10 $\mu$ M biotin-hBD3 or control buffer at 4°C overnight. The beads were spun down and washed with lysis buffer 10 times and protein bound to the beads was extracted using NuPAGE LDS Sample Buffer and analyzed by western blot.

### Western blot

Supernatants and cell lysates were loaded on Bolt Bis-Tris Plus gels (Life Technologies), and transferred to PVDF membranes using the iBlot system (Thermo Fisher). Membranes were blocked and incubated with primary antibodies at 4°C overnight.

For co-IP analysis in [Figure 1F](#), rabbit anti-biotin (Abcam, 1:1000) was used to detect biotin-hBD3, rabbit anti-GFP (Thermo Fisher, 1:1000) was used for Mrgpra2b-GFP or MRGPRX4-GFP. For [Figure 7E](#), goat anti mouse IL-1 $\beta$  (R&D systems, 1:1000) was used to detect pro-IL-1 $\beta$  (31kDa), rabbit anti-mouse cleaved-IL-1 $\beta$  (Cell Signaling Technology, 1:500) was used to detect mature IL-1 $\beta$  (17kDa), goat anti-Actin beta (Abcam, 1:1000) was used as loading control. On the next day, secondary antibodies (R&D HRP conjugated anti-goat or anti-rabbit, 1:1000) were applied, followed by SuperSignal™ West Pico Substrate solution (Thermo Scientific) and the blots were imaged on a chemiluminescent blot imager (Cytiva).

### K<sub>D</sub> determination by flow cytometry

Control HEK cells or HEK cells stably expressing Mrgpra2b-GFP were incubated with control medium (complete DMEM) or various concentrations of biotin-hBD3 peptides for three hours at 37°C. Cells were washed in PBS five times, stained using PE-anti-biotin antibody (Biolegend) in FACS buffer for 30 minutes. Mean fluorescent intensity of PE for each sample was measured by flow cytometry.

### Protein quantification by ELISA

Snap-frozen skin tissues were weighed and homogenized in PBS using a Pro200 Series homogenizer (Pro Scientific). Elastase and Myeloperoxidase (MPO), S100A8/A9, CXCL2 and IL-1 $\beta$  were measured using ELISA DuoSets (R&D Systems) according to manufacturer's instructions. mBD14 was measured using an ELISA kit from Abxbexa. The same samples were measured for multiple factors.

### 16S sequencing

Microbiome samples were collected from a 2 cm  $\times$  4 cm area on mouse back skin using sterile cotton swabs (Epicentre) pre-moistened with lysis buffer (20 mmol/L Tris [pH 8.0], 2 mmol/L EDTA and 1.2% Triton X-100) and immediately frozen in 250  $\mu$ L of lysis buffer in -80°C. All samples were submitted on a 96 well plate to the University of Michigan Microbial Systems Molecular Biology Laboratory for Illumina 16S rDNA gene sequencing. Briefly, the V4 region of 16S RNA were amplified by PCR, barcoded and sequenced on an Illumina MiSeq platform. Initial informatics analyses were performed by the Johns Hopkins SKCCC Experimental and Computational Genomics Core using the Qiime2 platform ([Bolyen et al., 2019](#)). The GreenGenes database was used as reference for taxonomic classification and alpha and beta diversity metrics were computed in Qiime2. Principal coordinate analysis (PCoA) of beta diversity was performed and visualized in R. For neutrophil depletion ([Figures S3C–S3G](#)), mice were intraperitoneally treated with 250 $\mu$ g of anti-Ly6g antibody or isotype control diluted in 100 $\mu$ L PBS every other day for 2 weeks. Skin swabs were collected as described above.

### Histology

Skin samples were fixed in 4% paraformaldehyde (PFA) in PBS overnight and submitted to the Johns Hopkins Oncology Tissue Services where they were embedded in paraffin, sliced into 4  $\mu$ m sections, mounted and stained with hematoxylin and eosin (H&E). Gram stain was performed using the Gram Staining Kit (Sigma Aldrich) according to manufacturer's instructions. For immunofluorescence labeling, paraffin sections were deparaffinized, underwent heat-mediated antigen retrieval in either Trilogy buffer (Cell Marque) or Tris-EDTA buffer (10mM Tris Base, 1 mM EDTA Solution, 0.05% Tween 20, pH 9.0), blocked in blocking buffer (PBS with 10% goat serum) for 1 hour at room temperature, and then incubated at 4°C overnight with 1  $\mu$ g/mL rabbit anti-mBD14, rat anti-mouse Ly6G or rabbit anti-*S.aureus* primary antibodies in blocking buffer. The next day, sections were incubated for 1 hour at room temperature with 1  $\mu$ g/mL of either AlexaFluor-488 goat anti-rabbit IgG (ThermoFisher, for mBD14 staining), AlexaFluor-488 goat anti-rat IgG (ThermoFisher, for Ly6G staining) or AlexaFluor-594 goat anti-rabbit IgG (ThermoFisher, for *S. aureus* staining). All slides were washed and mounted with Fluoromount-G with DAPI (ThermoFisher). All microscopy were performed on a Keyence BZ-X710 microscope (Keyence) and analyzed with Image J (National Institutes of Health Research Services Branch).

### RNA extraction and quantification

Snap-frozen skin tissue or purified cells were homogenized in Trizol and RNA was extracted using a Direct-zol RNA Miniprep kit (Zymo Research) following manufacturer's instructions. mRNA was reverse-transcribed into cDNA using a SuperScript III kit (Invitrogen) followed by RNase digestion. Quantitative PCR (qPCR) was performed using an EagleTaq mastermix (Roche) and Taqman gene expression probes (Thermo Fisher) corresponding to each gene of interest on a StepOnePlus RT-PCR system (Applied Biosystems).

Gene expression was normalized to *Actb* using the  $\Delta$ Ct method. The same samples were measured for multiple mRNAs. RT-PCR of *Mrgpra2* and *Gapdh* was done using primers listed in the [key resources table](#).

### RNA sequencing

Total RNA was extracted from naïve or *S. aureus*-infected skin (24 hours post intradermal injection of  $3 \times 10^7$  CFU USA300 LAC::lux) using Trizol-chloroform and purified using the Qiagen RNeasy Plus Mini kit. 6 control samples and 6 SA (*S. aureus*-infected) samples of each genotype (WT, *Def* cKO and *Mrgpra2* dKO) were submitted to the Johns Hopkins Transcriptomics and Deep Sequencing Core. Libraries were constructed using the Illumina Stranded Total RNA Prep Ligation with Ribo-Zero Plus kit with standard protocol and sequenced on an Illumina NovaSeq 6000 system. Reads were mapped to the mm10 reference mouse genome with STAR using default parameters. Counts were quantified and normalized to fragments per kilobase per million mapped reads (FPKM) using Partek Flow, and one-way ANOVA tests were run between experimental groups. Data were visualized using GraphPad Prism 9.

### Mouse models of *S. aureus* skin infection and quantification by IVIS

For intradermal *S. aureus* infections, mice were shaved on the back and inoculated with an intradermal injection of mid-logarithmic growth phase bioluminescent *S. aureus* CA-MRSA strain USA300 LAC::lux as previously described ( $3 \times 10^7$  CFUs/100  $\mu$ L PBS) using 29-gauge insulin syringes (Dillen et al., 2018). For the epicutaneous swab infection model,  $10^9$  CFUs/50  $\mu$ L PBS of CA-MRSA strain SF8300 was dropped on the shaved back skin and spread into a 2 cm  $\times$  2 cm area using a pre-moistened cotton swab (Malhotra et al., 2016). Digital photographs (Nikon Coolpix 5400) of infected skin were taken and lesion sizes were quantified using Image J (National Institutes of Health Research Services Branch) with a millimeter ruler as a reference. For in vivo bioluminescence imaging (BLI) quantification, mice were anesthetized via inhalation of isoflurane (2%), and imaged on a Lumina III IVIS (PerkinElmer); total flux (photons/s) was measured within a  $1 \times 10^3$ -pixel circular region of interest using Living Image software (PerkinElmer). For rescue experiments, hBD3 (Anaspec) was dissolved in PBS to 100  $\mu$ M and 50  $\mu$ L of either hBD3 or PBS was intradermally injected at the infection sites 6 hours post-*S. aureus* injection. For experiments in [Figures 7G–7I](#), IL-1 $\beta$  and CXCL2 (100ng each, R&D) were co-injected with *S. aureus* (Miller et al., 2007).

### Adoptive transfer of neutrophils

Bone marrows were taken from WT animals under sterile conditions and neutrophils were selected using the MACS Neutrophil Isolation Kit (Miltenyi Biotec). Purified neutrophils were resuspended in PBS and  $5 \times 10^6$  cells/100 $\mu$ L were retro-orbitally injected into *Mrgpra2* dKO animals 2 hour before *S. aureus* infection.

### Flow cytometry

10-mm skin punch biopsies were minced and digested in 3 mL RPMI containing 100  $\mu$ g/mL DNase I (Sigma-Aldrich) and 1.67 Wunsch units/mL Liberase TL (Roche) for one hour at 37  $^{\circ}$ C on a rotor wheel. Single cell suspensions were generated by passing digested skin samples through 100- $\mu$ m cell strainers and washed in RPMI and PBS. Live versus Dead cells were stained using Live/Dead Fixable Aqua Dead Cell Stain Kit (Thermo Fisher). Cells were treated with CD16/CD32 Fc Block (S17011E, Biolegend) for 10 min before incubation with the antibody cocktail: CD45-APC/Cy7 (30-F11, Biolegend), CD11b-PE/Dazzle594 (M1/70, Biolegend), CD11c-PE/Cy7 (N418, Biolegend), Ly6C-APC (HK1.4, Biolegend), Ly6G-BV421 (1A8, Biolegend), F4/80-BV605 (BM8, Biolegend) and SiglecF-BB515 (E50-2440, BD Bioscience). Data were collected using a CytoFLEX LX (Beckman Coulter) and analyzed using FlowJo (BD). Neutrophils were gated as live CD45 $^+$ CD11b $^+$ Ly6G $^+$ .

### Isolation and stimulation of bone marrow neutrophils

Neutrophils were isolated from bone marrow by negative selection using the Neutrophil Isolation Kit with magnetic-activated cell sorting (MACS) columns (Miltenyi Biotec) following manufacturer's instructions. Purity of neutrophils after selection was validated by flow cytometry (>90%).  $10^5$ - $10^6$  cells were used for each condition. To measure elastase and MPO release,  $2 \times 10^5$  cells were resuspended in RPMI medium on a round-bottom 96 well plate and incubated with 0, 1, 5 or 10  $\mu$ M hBD3 peptide (Anaspec, dissolved in RPMI) or 10  $\mu$ M mBD14 (Dr. Wuyuan Lu) for one hour and the supernatant was analyzed for elastase and MPO concentrations using DuoSet ELISA kits (R&D Systems). Chemotaxis was measured using Boyden chambers with 8 micron filters.  $1 \times 10^5$  cells were seeded in the upper chamber and the lower chambers contained control medium, migration inducer (Abcam) or 10  $\mu$ M hBD3. The cells were incubated at 37 $^{\circ}$ C for 4 hours and the numbers of cells in the lower chamber were counted. For the measurement of NETosis,  $10^5$  cells were seeded in a flat-bottom 96 well plate and incubated with control medium, 10 nM PMA, 10  $\mu$ M Nigericin, 1mM ATP or 10  $\mu$ M hBD3 for 4 hours. SYTOX Orange dye (ThermoFisher, 0.25  $\mu$ M) was added to each well, incubated for 5 min and fluorescence was measured at excitation and emission wavelengths of 540 nm and 580 nm on Flex Station 3 (Molecular Devices) (Jiang et al., 2017). Reactive oxygen species (ROS) generation was measured using a Neutrophil/Monocyte Respiratory Burst Assay Kit (Cayman) following manufacturer's instructions.

To assay IL-1 $\beta$  and CXCL2 release, cells were pre-incubated with 1  $\mu$ g/mL *S. aureus* lipoteichoic acid (LTA, Invivogen) for 2 hours before hBD3 or mBD14 were added at final concentrations of 10  $\mu$ M. Another 2 hours later, supernatants were taken, and the remaining cells were lysed in RIPA buffer (Sigma). IL-1 $\beta$  and CXCL2 concentrations in the supernatants and cell lysates were assayed using DuoSet ELISA (R&D Systems). ATP (5 mM) was used as a positive control. For pharmacological inhibitions ([Figures 7E and 7F](#)),

Q-VD-Oph (R&D Systems) or YM254890 (Tocris) were added together with LTA to final concentrations of 10 $\mu$ M. Proteome profiler array (R&D Systems) was performed following manufacturer's instructions.

#### **QUANTIFICATION AND STATISTICAL ANALYSIS**

Image quantifications were performed using ImageJ (NIH). All statistical analyses were performed using Prism 9 (GraphPad). Single comparisons were made using two-tailed unpaired Student's t test. Data for multiple comparisons were analyzed using one-way or two-way ANOVA as specifically indicated in the figure legends. All data are presented as mean  $\pm$  standard error of the mean (SEM) and values of  $*p < 0.05$  were considered statistically significant.